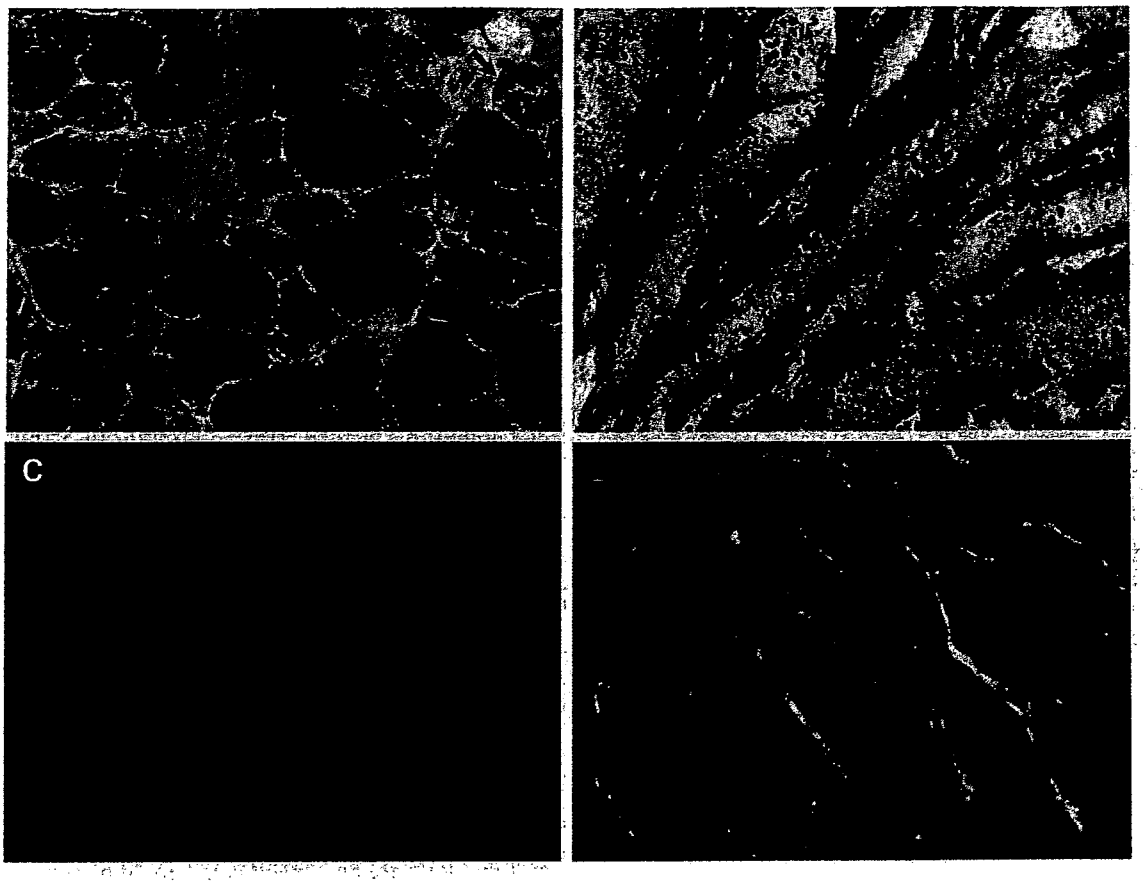

Figure 10. The diaphragm and cardiac muscles are likewise involved in the $Gne^{(-/-)}$h*GNE*V572L-Tg mice. (**A**) Modified Gomori trichrome section of a 48-week-old male $Gne^{(-/-)}$h*GNE*V572L-Tg. Note the presence of endomysial fibrosis and fiber with RV. (**B**) Hematoxylin and eosin sections from a 54-week-old female $Gne^{(-/-)}$h*GNE*V572L-Tg showing marked fibrosis. (**C**) Amyloid deposition (Amyloid β 1–42) is seen in the cardiomyocytes of the same mouse in (B). (**D**) HE section of cardiac muscle from a 42-week-old male $Gne^{(-/-)}$h*GNE*V572L-Tg reveals that RVs are occasionally seen in cardiomyocytes.

pathomechanism has largely been enigmatic up to this time, but unfolding and misfolding of proteins most probably play a role. Previous reports have alluded to the role of sialic acid in proper folding of proteins (35–37). The ultimate fate of aggregated, misfolded glycoproteins is degradation, hence the activation of UPR is expected, which could explain the presence of ubiquitin signals in the myofibers of the $Gne^{(-/-)}$ h*GNE*V572L-Tg mice and upregulation of ubiquitin and proteasome in DMRV/h-IBM myofibers (38).

The implication of amyloid deposition in the formation of RVs in both DMRV/h-IBM and s-IBM (39) is supported by our finding that the occurrence of amyloid inclusions in the myofibers preceded RV formation. Amyloid itself has been shown *in vitro* to block the degradation of ubiquitinated proteins by inhibiting proteasome activity (40), hence its accumulation may not only lead to cytotoxicity, but also may further aggravate protein misfolding. In addition, it has been clarified that overproduction of amyloid can induce tau hyperphosphorylation and decrease its solubility (41). Sialylation and glycosylation of amyloid precursor protein, which contains both *O*- and *N*-glycans, appear to be important for its proteolytic processing, secretion and metabolism (42–45). Interference with the formation of *N*-linked glycans resulted in a decrease in secreted AβPP and an increase in the level of the cellular form of the protein, which has a higher propensity to form amyloid β peptide (42,46). Although amyloid fibrils were the structure previously considered to be cytotoxic, there is current experimental evidence that pre-amyloid oligomeric complexes or aggregates, either diffuse or in a protofibril stage, can be very cytotoxic (47). The presence of dense deposits in areas with relatively preserved myofibrillar architecture on electron microscopy strongly suggest that deposition of amyloid and amyloid-like structures pre-date RV formation.

Because DMRV/h-IBM patients do not present, in general, with symptoms reflecting involvement of the respiratory system, it is assumed that the diaphragm is relatively spared in this myopathy. In the $Gne^{(-/-)}$h*GNE*V572L-Tg mice, it is clear that the diaphragm can be involved, despite the absence of overt respiratory difficulties. The presence of pathological findings in the sacrificed mice, and not only in the ones that died suddenly, may suggest that the presence of RVs *per se*, may not correlate with severity in phenotype, with respect to involvement of diaphragm. A more sensitive method of assessing the respiratory status of these mice, *vis-à-vis* a plain observation, might be helpful in clarifying the extent to which respiratory system is involved. Our results suggest that careful evaluation of respiratory and cardiovascular functions is logical and warranted in human patients.

In the *Gne*$^{(-/-)}$h*GNE*V572L-Tg mice, we have seen RVs in the cardiac muscles obtained from a couple of mice, clearly supporting the presence of cardiac involvement in DMRV/h-IBM. It has always been reported that DMRV involves primarily skeletal muscles but recently, however, it is being recognized that other organs may likewise be involved. For example, cardiac involvement is not very rare as it is seen in 18% of patients, with a spectrum of manifestations ranging from an incomplete right bundle-branch block to a fatal arrhythmia which led to sudden death (25,26). Sialic acid was shown to be an important component on the surface of heart muscle cells, because its removal reduced the cell surface negative charge by 25% (48) and produced a large increase in cardiac myocyte Ca^{2+}, followed by marked cell contracture (49), emphasizing the importance of negatively charged sialic acid-containing gangliosides in the maintenance of cardiac cell physiological Ca^{2+} permeability. More importantly, it has been demonstrated that in myocardial cells, desialylation of cells by neuraminidase treatment causes aberrant electrical activity (50), and may lead to arrhythmia (51).

In conclusion, we have generated the first mouse model of DMRV/h-IBM, which resembles the clinical, pathological and biochemical features of the disease in humans. The *Gne*$^{(-/-)}$h*GNE*V572L-Tg mouse is a concrete evidence that mutations in the *GNE* are causative of DMRV/h-IBM. Indeed, these DMRV/h-IBM mice will be a valuable tool to search for further clues in unraveling the pathomechanism of this myopathy. As we have clearly documented in these mice, hyposialylation plays a key role in the pathogenesis of DMRV/h-IBM, and is of paramount importance in considering therapeutic trials.

MATERIALS AND METHODS

Generation of *Gne* knockout mice

The *Gne* knockout mice [*Gne*$^{(-/-)}$] was produced in inGenious Targeting Laboratory (New York, NY, USA). The 17 kb mouse genomic DNA fragment, containing exons 3–5, was cloned from the mouse 129Sv/Ev lambda genomic library. The Neo cassette that was inserted replaced the 1.4 kb upstream of exon 3, exon 3 and 124 bp downstream of exon 3 (Fig. 1). The resulting targeting vector was linearized by *Not*I, purified and then transfected by electroporation into ES cells. Positive clones after neomycin selection were identified using PCR (primer sequences available upon request).

Generation of h*GNE*V572L-Tg

The cDNA for *GNE* mutant was obtained by reverse transcribed-PCR from skeletal muscle RNA of a DMRV patient with the V572L mutation and cloned into pCR-Blunt vector (Invitrogen, Carlsbad, CA, USA), as described previously (17). Cloned cDNA was sequenced by ABI cycle-sequencing procedures using an ABI 3100 (Applied Biosystems, Foster City, CA, USA). The *Xho*I fragment containing *GNE* mutant cDNA was excised and inserted into pCAGGS vector in which gene expression is driven by a CAG promoter (52). *loxP* sequences were introduced to flank the cDNA insert. *Sal*I fragment was purified and injected into C57BL/6 oocytes and subsequently transplanted into recipient mice. Founders were bred to WT C57BL/6 females to check for germline transmission, which was confirmed by PCR analyses on genomic DNA.

Production of *Gne*$^{(-/-)}$h*GNE*V572L-Tg

To maintain the same copy number of transgene, stringent measures were taken in generating mice. The h*GNE*V572L-Tg mouse was crossbred to *Gne* heterozygous mouse [*Gne*$^{(+/-)}$] to create a *Gne*$^{(+/-)}$ mouse that carried the human *GNE* [*Gne*$^{(+/-)}$h*GNE*V572L-Tg]. The latter was then mated with a *Gne*$^{(+/-)}$ mouse, to obtain a mouse that harbors the human V572L mutated *GNE* in a *Gne* knockout background.

For genotyping, DNA was isolated from mouse tails. *Gne* mice genotyping was carried out using PCR analysis on tail genomic DNA with the following primers: Neo, WT3 and S2 (primer sequences available upon request). Further, DNA was digested with *Bam*HI, subjected to Southern blotting and then analyzed by hybridization to a 500 bp probe.

For transgenic mice, the following oligonucleotides were used to amplify a 318 bp segment found specifically in human *GNE*: 1186F, CTTCAAGAGCCACTGCAAA; 1504R, CAATTCCTTCCCGAGGATT.

mRNA expression and determination of copy number

Mouse skeletal muscles, heart, brain, spleen and liver were dissected and rapidly frozen in liquid-nitrogen. Total RNA was extracted from cryostat sections of tissues with TRIzol (Invitrogen) following the manufacturer's protocol. First-strand cDNA was synthesized from RNA by reverse transcription using the Superscript RNase H$^-$ Reverse Transcriptase (Invitrogen) and random hexamers. Gene expression was measured by quantitative real-time PCR in i-Cycler IQ system (Bio-Rad Laboratories, Hercules, CA, USA). Primers (1186F and 1504R) were used to span exon–intron junctions to prevent amplification of genomic DNA. Relative quantification of gene expression was determined by comparison of threshold values as suggested by the manufacturer. All results were normalized with respect to Gapdh expression.

Transgene copy number was determined by the i-Cycler IQ system using the SYBR Green reagent kit according to the manufacturer's instructions. Triplicate samples of tail DNA from transgenic mice of each line were analyzed concurrently against a standard curve of scaled concentrations of an external standard. Primers were designed to amplify the transgene h*GNE*V572L and endogenous *Gne*; twice the ratio of the h*GNE*V572L/*Gne* amplicons was interpreted as copy number.

Sialic acid measurement

The bound sialic acids from the serum and pieces of different tissues were released using 20 mM sulfuric acid hydrolysis for 1 h at 80°C. Free sialic acids were then derivitized with 1, 2-diamino-4, 5-methylenedioxybenzene and analyzed by reverse-phase HPLC fluorescence detection as described previously (53). The eluant was monitored by fluorescence and

Table 1. Antibodies used in the study

Antibody	Manufacturer	Type	Dilution
AβPP (6E10)	Chemicon International Inc., Temecula, CA, USA	Mouse monoclonal	1:1000
Aβ 1–40	Chemicon	Rabbit polyclonal	1:100
Aβ 1–42	Chemicon	Rabbit polyclonal	1:100
Aβ oligomer (A11)	Chemicon	Rabbit polyclonal	1:1000
Human beta site APP cleaving enzyme	Alpha Diagnostic International	Rabbit polyclonal	1:100
Caveolin 3	Transduction Laboratories, Lexington, KY, USA	Rabbit polyclonal	1:400
α-dystroglycan (VIA4-1)	Upstate Cell Signaling Solutions, Lake Placid, NY, USA	Mouse monoclonal	1:100
β-dystroglycan	A gift from Dr Ejiro Ozawa	Rabbit polyclonal	1:200
Grp94 (9G10)	Stressgen Biotechnologies, Calgary, Canada	Rat monoclonal	1:30
LAMP-1 (25)	BD Transduction Laboratories, Lexington, KY, USA	Mouse monoclonal	1:100
LAMP-2A	A gift from Dr Fumitaka Oyama	Rabbit polyclonal	1:100
LC3	A gift from Dr Tamotsu Yoshimori	Rabbit polyclonal	1:200
NCAM (123C3)	Santa Cruz Biotechnology Inc.	Mouse monoclonal	1:100
α-sarcoglycan (Ad1/20A6)	Novocastra Laboratories Ltd.	Mouse monoclonal	1:100
β-sarcoglycan (βSarc/5B1)	Novocastra Laboratories Ltd.	Mouse monoclonal	1:100
polyUbiquitin (FK1)	Biomol International	Mouse monoclonal	1:500
Neurofilament (SM-31)	Sternberg Monoclonals Inc., MD, USA	Mouse monoclonal	1:1000
Neurofilament (SM-310)	Sternberg Monoclonals Inc., MD, USA	Mouse monoclonal	1:1000
tau C	A gift from Dr Fumitaka Oyama	Rabbit polyclonal	1:1000

measured by comparison with Neu5Ac and Neu5Gc standards (from 0.05 nmol/μl to 5 nmol/μl). Total protein from tissues was measured using the Bio-Rad Protein Assay (Bio-Rad Laboratories) according to the manufacturer's protocol.

General assessment for motor strength and fatigability

Whole-animal strength and fatigability were measured according to a test procedure (here referred to as rod-climbing test) previously reported (54). In brief, this test required the mice to pull themselves on top of a suspended rod (3 mM in diameter). The measurement of muscle weakness was based on the mean percentage of passes over 15 trials of the test in a 3-min period. Fatigability was assessed as the average pass rate over time for each group of mice. The test was repeated at least three times after a 2-week period.

Histopathological and histochemical analyses

Fresh specimens from individual skeletal and cardiac muscles were snap-frozen in liquid-nitrogen-cooled isopentane and stored at −80°C until further processing. We stained frozen sections (6 μm) of transversal skeletal and cardiac muscles with a battery of histochemical stains including hematoxylin and eosin, modified Gomori trichrome and acid phosphatase. Sections were analyzed by light microscopy. We performed Congo red staining in 10 μm cryosections following the Putchler's modification, and viewed sections under light microscope and conventional fluorescence microscope using Texas-red filters (39). For immunohistochemical analysis, tissue sections were fixed either in acetone or paraformaldehyde, depending on the primary antibody used, and blocked with 5% normal serum and 2% bovine serum albumin in phosphate-buffered saline. The primary antibodies used are listed in Table 1. We used several antibodies which recognize amyloidβ. 6E10, which is a human-specific antibody, but also reacts to murine tissue when the amyloid burden is high, primarily recognizes AβPP (residues 1–16) after α-secretase cleavage. It also recognizes, in addition, C99 fragment and amyloid β peptides (1–40 and 1–42) which have been shown to be prone to aggregation. The anti-oligomeric antibody (A11) is specific to the oligomeric structure of β amyloid peptides. The following secondary antibodies were used appropriately: anti-goat IgG F (ab′)-2-fragment, FITC conjugated (EY Laboratories, San Mateo, CA, USA); anti-rabbit IgG (H + L), Alexa Fluor conjugated (Molecular Probes, Eugene, OR, USA); anti-mouse IgG1, FITC conjugated (Sanbio/Monosan, Uden, The Netherlands). Images were collected and analyzed with a laser scanning microscope (Olympus, Tokyo, Japan) with its appropriate software.

Morphometric analysis of fibers

Muscle cross sections were stained with rabbit polyclonal antibody against caveolin-3 followed by a fluorescent secondary antibody. Digital images from fluorescence signals were observed under a confocal microscope and the widest diameter was recorded for 600 or more fibers using Image-J software from the public domain NIH Image program (developed at the U.S. National Institutes of Health and available on the Internet at http://rsb.info.nih.gov/nih-image/). Results were analyzed using Statistics Software for Social Sciences (SPSS for Windows, Rel. 11.0.0. 2001, SPSS Inc., Chicago) software.

Electron microscopy

The muscle specimens were immediately fixed for 2 h in 2.5% cold glutaraldehyde with 0.1 M cacodylate buffer, pH 7.3. After washing in cacodylate buffer, the specimens were post-fixed in 1% osmium tetroxide in the same buffer, dehydrated with graded series of ethanol and embedded in Epon. Semithin sections (0.5 μm) were stained with toluidine blue alkaline. Ultrathin sections were stained with uranyl acetate, citrated and observed with a H-600 electron microscope (Hitachi, Tokyo, Japan) at 75 kV.

Serum CK

Blood samples were obtained either by inferior vena cava aspiration, or careful collection from mouse tail. Total CK activity was measured by a spectrophotometric assay employing a commercial kit (CPK-L Determiner, Kyowa MEDEX, Tokyo, Japan). For confirmation, CK isoforms were electrophoretically analyzed using Titan Gel CK Isozyme kit (Helena Laboratories, Beaumont, TX, USA) following the manufacturer's protocol.

Statistical analysis

Data were entered in SPSS version 11.0 and were analyzed by computation of the frequency and the mean ± SD and/or percentage. The data were then subjected to a univariate analysis (Fisher's exact test), Student's *t*-test, Wilcoxon paired test, ANOVA or Mann–Whitney *U* test, log-rank test or multiple regression analysis, whichever was appropriate. *P*-values less than 0.05 were considered to be statistically significant.

ACKNOWLEDGEMENTS

The authors thank the following persons for their invaluable support and assistance: Yoko Keira, Genri Kawahara, Mari Okada and Kumiko Murayama. This study is supported by the 'Research on Psychiatric and Neurological Diseases and Mental Health' from Health and Labour Sciences Research Grants; the 'Research on Health Sciences focusing on Drug Innovation' from the Japanese Health Sciences Foundation; the 'Research Grant (16B-2, 17A-10) for Nervous and Mental Disorders' from the Ministry of Health, Labour and Welfare; and the Program for Promotion of Fundamental Studies in Health Sciences of the National Institute of Biomedical Innovation (NIBIO).

Conflict of Interest statement. None declared.

REFERENCES

1. Nonaka, I., Sunohara, N., Ishiura, S. and Satoyoshi, E. (1981) Familial distal myopathy with rimmed vacuole and lamellar (myeloid) body formation. *J. Neurol. Sci.*, **51**, 141–155.
2. Argov, Z. and Yarom, R. (1984) 'Rimmed vacuole myopathy' sparing the quadriceps. A unique disorder in Iranian Jews. *J. Neurol. Sci.*, **64**, 33–43.
3. Nonaka, I., Noguchi, S. and Nishino, I. (2005) Distal myopathy with rimmed vacuoles and hereditary inclusion body myopathy. *Curr. Neurol. Neurosci. Rep.*, **5**, 61–65.
4. Ikeuchi, T., Asaka, T., Saito, M., Tanaka, H., Higuchi, S., Tanaka, K., Saida, K., Uyama, E., Mizusawa, H., Fukuhara, N. *et al.* (1997) Gene locus for autosomal recessive distal myopathy with rimmed vacuoles maps to chromosome 9. *Ann. Neurol.*, **41**, 432–437.
5. Mitrani-Rosenbaum, S., Argov, Z., Blumenfeld, A., Seidman, C.E. and Seidman, J.G. (1996) Hereditary inclusion body myopathy maps to chromosome 9p1-q1. *Hum. Mol. Genet.*, **5**, 159–163.
6. Nishino, I., Noguchi, S., Murayama, K., Driss, A., Sugie, K., Oya, Y., Nagata, T., Chida, K., Takahashi, T., Takusa, Y. *et al.* (2002) Distal myopathy with rimmed vacuoles is allelic to hereditary inclusion body myopathy. *Neurology*, **59**, 1689–1693.
7. Eisenberg, I., Avidan, N., Potikha, T., Hochner, H., Chen, M., Olender, T., Barash, M., Shemesh, M., Sadeh, M., Grabov-Nardini, G. *et al.* (2001) The UDP-*N*-acetylglucosamine 2-epimerase/*N*-acetylmannosamine kinase gene is mutated in recessive hereditary inclusion body myopathy. *Nat. Genet.*, **29**, 83–87.
8. Keppler, T., Hinderlich, S., Langner, J., Scwartz-Albiez, R., Reutter, W. and Pawlita, M. (1999) UDP-GlcNAc 2-epimerase: a regulator of cell surface sialylation. *Science*, **284**, 1372–1376.
9. Eisenberg, I., Grabov-Nardini, G., Hochner, H., Korner, M., Sadeh, M., Bertorini, T., Bushby, K., Castellan, C., Felice, K., Mendell, J. *et al.* (2003) Mutations spectrum of *GNE* in hereditary inclusion body myopathy sparing the quadriceps. *Hum. Mutat.*, **21**, 99.
10. Argov, Z., Eisenberg, I., Grabov-Nardini, G., Sadeh, M., Wirguin, I., Soffer, D. and Mitrani-Rosenbaum, S. (2003) Hereditary inclusion body myopathy: the Middle Eastern genetic cluster. *Neurology*, **60**, 1519–1523.
11. Tomimitsu, H., Shimizu, J., Ishikawa, K., Ohkoshi, N., Kanazawa, I. and Mizusawa, H. (2004) Distal myopathy with rimmed vacuoles (DMRV): new *GNE* mutations and splice variant. *Neurology*, **62**, 1607–1610.
12. Kim, B.J., Ki, C.S., Kim, J.W., Sung, D.H., Choi, Y.C. and Kim, S.H. (2006) Mutation analysis of the *GNE* gene in Korean patients with distal myopathy with rimmed vacuoles. *J. Hum. Genet.*, **51**, 137–140.
13. Ro, L.S., Lee-Chen, G.J., Wu, Y.R., Lee, M., Hsu, P.Y. and Chen, C.M. (2005) Phenotypic variability in a Chinese family with rimmed vacuolar distal myopathy. *J. Neurol. Neurosurg. Psychiatry*, **76**, 752–755.
14. Broccolini, A., Ricci, E., Cassandrini, D., Gliubizzi, C., Bruno, C., Tonoli, E., Silvestri, G., Pescatori, M., Rodolico, C., Sinicropi, S. *et al.* (2004) Novel *GNE* mutations in Italian families with autosomal recessive hereditary inclusion-body myopathy. *Hum. Mutat.*, **23**, 632.
15. Liewluck, T., Pho-Iam, T., Limwongse, C., Thongnoppakhun, W., Boonyapisit, K., Raksadawan, N., Murayama, K., Hayashi, Y.K., Nishino, I. and Sangruchi, T. (2006) Mutation analysis of the *GNE* gene in distal myopathy with rimmed vacuoles (DMRV) patients in Thailand. *Muscle Nerve*, Epub ahead of print.
16. Amouri, R., Driss, A., Murayama, K., Kefi, M., Nishino, I. and Hentati, F. (2005) Allelic heterogeneity of *GNE* gene mutation in two Tunisian families with autosomal recessive inclusion body myopathy. *Neuromuscul. Disord.*, **15**, 361–363.
17. Noguchi, S., Keira, Y., Murayama, K., Ogawa, M., Fujita, M., Kawahara, G., Oya, Y., Imazawa, M., Goto, Y., Hayashi, *et al.* (2004) Reduction of UDP-*N*-acetylglucosamine 2-epimerase/*N*-acetylmannosamine kinase activity and sialylation in distal myopathy with rimmed vacuoles. *J. Biol. Chem.*, **279**, 11402–11407.
18. Salama, I., Hinderlich, S., Shlomai, Z., Eisenberg, I., Krause, S., Yarema, K., Argov, Z., Lochmuller, H., Reutter, W., Dabby, R. *et al.* (2005) No overall hyposialylation in hereditary inclusion body myopathy myoblasts carrying the homozygous M712T GNE mutation. *Biochem. Biophys. Res. Commun.*, **328**, 221–226.
19. Hinderlich, S., Salama, I., Eisenberg, I., Potikha, T., Mantey, L.R., Yarema, K.J., Horstkorte, R., Argov, Z., Sadeh, M., Reutter, W. *et al.* (2004) The homozygous M712T mutation of UDP-*N*-acetylglucosamine 2-epimerase/*N*-acetylmannosamine kinase results in reduced enzyme activities but not in altered overall cellular sialylation in hereditary inclusion body myopathy. *FEBS Lett.*, **566**, 105–109.
20. Schwarzkopf, M., Knobeloch, K.P., Rohde, E., Hinderlich, S., Wiechens, N., Lucka, L., Horak, I., Reutter, W. and Horstkorte, R. (2002) Sialylation is essential for early development in mice. *Proc. Natl Acad. Sci. USA*, **99**, 5267–5270.
21. Mirabella, M., Alvarez, R.B., Bilak, M., Engel, W.K. and Askanas, V. (1996) Difference in expression of phosphorylated tau epitopes between sporadic and hereditary inclusion-body myopathies. *J. Neuropathol. Exp. Neurol.*, **55**, 774–786.
22. Akanas, V. and Engel, W.K. (2006) Inclusion-body myositis: a myodegenerative conformational disorder associated with Abeta, protein misfolding, and proteasome inhibition. *Neurology*, **66** (Suppl. 1), S39–S48.
23. Askanas, V. and Engel, W.K. (2003) Hereditary inclusion myopathies. In Rosenberg, R.N., Prusiner, S.B., DiMauro, S., Barchi, R.L. and Nestler, E.J. (eds), *The Molecular and Genetic Basis of Neurologic and Psychiatric Disease*, 3rd edn. Butterworth–Heinemann, Woburn, MA, USA, pp. 501–509.
24. Akanas, V. and Engel, W.K. (2003) Proposed pathogenic cascade of inclusion-body myositis: importance of amyloid-beta, misfolded proteins, predisposing genes, and aging. *Curr. Opin. Rheumatol.*, **15**, 734–744.
25. Horstkorte, R., Nöhring, S., Wiechens, N., Schwarzkopf, M., Danker, K., Reutter, W. and Lucka, L. (1999) Tissue expression and amino acid sequence of murine UDP-*N*-acetylglucosamine-2-epimerase/*N*-acetylmannosamine kinase. *FEBS J.*, **260**, 923–927.

26. Ishii, A., Hagiwara, Y., Saito, Y., Yamamoto, K., Yuasa, K., Sato, Y., Arahata, K., Shoji, S., Nonaka, I., Saito, I., Nabeshima, Y., Takeda, S. (1999) Effective adenovirus-mediated gene expression in adult murine skeletal muscle. *Muscle Nerve*, **22**, 592–599.
27. Kimpara, T., Imamura, T., Tsuda, T., Sato, K. and Tsuburaya, K. (1993) Distal myopathy with rimmed vacuoles and sudden death—report of two siblings. *Rinsho Shinkeigaku*, **33**, 886–890.
28. Nishino, I., Malicdan, M.C., Murayama, K., Nonaka, I., Hayashi, Y.K. and Noguchi, S. (2005) Molecular pathomechanism of distal myopathy with rimmed vacuoles. *Acta Myol.*, **24**, 80–83.
29. Sugarman, M., Kitazawa, M., Baker, M., Caiozzo, V.J., Querfurth, H.W. and LaFerla, F.M. (2006) Pathogenic accumulation of APP in fast twitch muscle of IBM patients and a transgenic model. *Neurobiol. Aging*, **27**, 423–432.
30. Post, J.A. (1992) Removal of sarcolemmal sialic acid residues results in a loss of sarcolemmal functioning and integrity. *Am. J. Physiol.*, **263**, H147–H152.
31. Bennett, E., Urcan, M.S., Tinkle, S.S., Kozkowski, A. and Levinson, S. (1997) Contribution of sialic acid to the voltage dependence of sodium channel gating: a possible electrostatic mechanism. *J. Gen. Physiol.*, **109**, 327–343.
32. Nishino, I. (2003) Autophagic vacuolar myopathies. *Curr. Neurol. Neurosci. Rep.*, **3**, 64–69.
33. Askanas, V., Alvarez, R.B. and Engel, W.K. (1993) β-Amyloid precursor epitopes in muscle fibers of inclusion body myositis. *Ann. Neurol.*, **34**, 551–560.
34. Askanas, V. and Engel, W.K. (1995) New advances in the understanding of sporadic inclusion-body myositis and hereditary inclusion-body myopathies. *Curr. Opin. Rheumatol.*, **7**, 486–496.
35. Ellis, R. and Pinheiro, T.J.T. (2002) Danger: misfolding proteins. *Nature*, **416**, 483–484.
36. Brooks, S.A., Dwek, M.V. and Schumacher, U. (2002) *Functional and Molecular Gycobiology*. BIOS Scientific Publishers Limited, Oxford, UK.
37. Helenius, A. and Aebi, M. (2004) Roles of *N*-linked glycans in the endoplasmic reticulum. *Annu. Rev. Biochem.*, **73**, 1019–1049.
38. Kumamoto, T., Fujimoto, S., Nagao, S., Masuda, T., Sugihara, R., Ueyama, H. and Tsuda, T. (1998) Proteasomes in distal myopathy with rimmed vacuoles. *Intern. Med.*, **37**, 746–752.
39. Askanas, V., Engel, W.K. and Alvarez, R.B. (1993) Enhanced detection of congo-red-positive amyloid deposits in muscle fibers of inclusion body myositis and brain of Alzheimer's disease using fluorescence technique. *Neurology*, **43**, 1265–1267.
40. Gregori, L., Hainfeld, J.F., Simon, M.N. and Goldbager, D. (1997) Binding of amyloid β protein to the 20S proteasome. *J. Biol. Chem.*, **272**, 58–62.
41. Wang, Y.P., Wang, X.C., Tian, Q., Yang, Y., Zhang, Q., Zhang, J.Y., Zhang, Y.C., Wang, Z.F., Wang, Q., Li, H. *et al.* (2006) Endogenous overproduction of β-amyloid induces tau hyperphosphorylation and decreases the solubility of tau in N2a cells. *J. Neural. Transm.*, Epub ahead of print.
42. McFarlane, I., Georgopoulou, N., Coughlan, C.M., Gillian, A.M. and Breen, K.C. (1999) The role of the protein glycosylation state in the control of cellular transport of the amyloid beta precursor protein. *Neuroscience*, **90**, 15–25.
43. Pahlsson, P. and Spitalnik, S.L. (1996) The role of glycosylation in synthesis and secretion of beta-amyloid precursor protein by Chinese hamster ovary cells. *Arch. Biochem. Biophys.*, **331**, 177–186.
44. Yazaki, M., Tagawa, K., Maruyama, K., Sorimachi, H., Tsuchiya, T., Ishiura, S. and Suzuki, K. (1996) Mutation of potential *N*-linked glycosylation sites in Alzheimer's disease amyloid precursor protein (APP). *Neurosci. Lett.*, **221**, 57–60.
45. Nakagawa, K., Kitazume, S., Oka, R., Maruyama, K., Saido, T.C., Sato, Y., Endo, T. and Hashimoto, Y. (2006) Sialylation enhances the secretion of neurotoxic amyloid-beta peptides. *J. Neurochem.*, **96**, 924–933.
46. Georgopoulou, N., McLaughlin, M., McFarlane, I. and Breen, K.C. (2001) The role of post-translational modification in beta-amyloid precursor protein processing. *Biochem. Soc. Symp.*, **67**, 23–36.
47. Tsai, B., Ye, Y. and Rapoport, T.A. (2002) Retro-translocation of proteins from the endoplasmic reticulum into the cytosol. *Nat. Rev. Mol. Cell Biol.*, **3**, 246–255.
48. Soeiro, M.N., Silva-Filho, F.C. and Meirelles, M.N. (1994) The nature of anionic sites and the endocytic pathway in heart muscle cells. *J. Submicrosc. Cytol. Pathol.*, **26**, 121–130.
49. Marengo, F.D., Wang, S.Y., Wang, B. and Langer, G.A. (1998) Dependence of cardiac cell Ca^{2+} permeability on sialic acid-containing sarcolemmal gangliosides. *J. Mol. Cell Cardiol.*, **30**, 127–137.
50. Woods, W.T., Inamura, K. and James, T.R. (1982) Electrophysiological and electron microscopic correlations concerning the effects of neuraminidase on canine heart cells. *Circ. Res.*, **50**, 228–231.
51. Ufret-Vincenty, C.A., Baro, D.J. and Santana, L.F. (2001) Differential contribution of sialic acid to the function of repolarizing K^+ currents in ventricular myocytes. *Am. J. Physiol. Cell Physiol.*, **281**, C464–C474.
52. Niwa, H., Yamamura, K. and Miyazaki, J. (1991) Efficient selection for high-expression transfectants with a novel eukaryotic vector. *Gene*, **108**, 193–199.
53. Hara, S., Yamaguchi, M., Takemori, Y., Nakamura, M. and Ohkura, Y. (1986) Highly sensitive determination of *N*-acetyl- and *N*-glycolylneuraminic acids in human serum and urine and rat serum by reversed-phase liquid chromatography with fluorescence detection. *J. Chromatogr.*, **377**, 111–119.
54. Keppler, O.T., Hinderlich, S., Langner, J., Schwartz-Albiez, R., Reutter, W. and Pawlita, M. (1999) UDP-GlcNAc 2-epimerase: a regulator of cell surface sialylation. *Science*, **284**, 1372–1376.

ELSEVIER

Brain & Development 29 (2007) 112–116

BRAIN & DEVELOPMENT
Official Journal of the Japanese Society of Child Neurology

www.elsevier.com/locate/braindev

Case Report

Familial reducing body myopathy

Maki Ohsawa [a,*], Teerin Liewluck [b], Katuhisa Ogata [c], Takahiro Iizuka [d], Yukiko Hayashi [b], Ikuya Nonaka [a], Masayuki Sasaki [a], Ichizo Nishino [b]

[a] *Department of Child Neurology, National Center Hospital for Mental, Nervous and Muscular Disorders, National Center of Neurology and Psychiatry (NCNP), Kodaira, Tokyo 187-8551, Japan*
[b] *Department of Neuromuscular Research, National Institute of Neuroscience, NCNP, Kodaira, Tokyo 187-8502, Japan*
[c] *Department of Neurology, National Center Hospital for Mental, Nervous and Muscular Disorders, NCNP, Kodaira, Tokyo 187-8551, Japan*
[d] *Department of Neurology, Kitasato University School of Medicine, Sagamihara, Kanagawa 228-8555, Japan*

Received 16 November 2005; received in revised form 22 June 2006; accepted 26 June 2006

Abstract

Reducing body myopathy (RBM) is a rare pathologically defined myopathy characterized by the presence of inclusion bodies which are abnormally stained by menadione–nitroblue–tetrazolium. The clinical symptoms vary widely as to the age of onset, disease progression and severity. Among the many reported patients, there have been only three families with this disorder, showing a manifold of clinicopathological features in each family. We report a fourth family with RBM affecting a boy and his mother. The proband (boy) began to have difficulty putting on his trousers at age 10 years and difficulty arising from a chair at 11 years. His spine was rigid. His mother, on the other hand, noticed foot-drop at the age 29, but the clinical course was rapidly progressive, and she was wheelchair-bound at 34 years. Both patients had generalized muscle weakness and atrophy and with mild CK elevation. Muscle pathology was characterized by the presence of atrophic fibers with reducing bodies in some areas. As these patients demonstrate, clinical symptoms in RBM are very variable, even within the same family. There are no specific clinical characteristics distinctive to RBM, thus further studies are necessary to characterize this disorder both clinically and pathologically.

Keywords: Reducing body myopathy; Familial; Mother and Son; Rapidly progressive

1. Introduction

Reducing body myopathy (RBM) is a group of heterogeneous disorders characterized pathologically by the presence of inclusion bodies that reduce nitroblue tetrazolium (NBT) in the absence of menadione as a substrate in the α-glycerophosphate dehydrogenase reaction. In 1972, Brooke and Neville initially described two unrelated girls with a severe congenital myopathy with reducing bodies [1]. The clinical spectrum of this disease is wide, showing different age of onset, course and severity of disease [2–10]. Although most of the cases have been sporadic, there have been three families with this disorder. Here, we report the fourth family with RBM and discuss the clinical and pathologic findings.

2. Patients and muscle pathology

2.1. Case history

The proband is an 11-year-old boy, the second of three children of a Japanese father and Filipino mother. Both his brothers were healthy except that the younger one had a history of Hirschsprung disease. Pregnancy

* Corresponding author. Tel.: +81 42 341 2711; fax: +81 42 344 6745.
E-mail address: mohsawa@ncnp.go.jp (M. Ohsawa).

0387-7604/$ - see front matter © 2006 Elsevier B.V. All rights reserved.
doi:10.1016/j.braindev.2006.06.010

and delivery were uneventful and psychomotor development was normal. Until 9 years of age, he could run faster than his classmates. At the age of 10 years and 5 months, he began to have difficulty putting on his trousers. One month after the onset, he developed foot-drop and began to fall frequently. Two months later, he had difficulty getting up from a sitting position. He could no longer run as fast as when he was 10 years old.

On physical examination, he had generalized muscle atrophy and weakness, especially around the shoulder, hip and anterior compartment of the lower legs. There was winging of the scapulae. Muscle weakness was slightly more marked on the left than the right. His spine was rigid on anteflexion and he had a lumbar lordosis. He was able to walk on his toes but not on his heels. Gowers' sign was positive. Deep tendon reflexes were diminished. Facial and extra-ocular muscles were normal. There were no fasciculations, calf muscle hypertrophy or pes cavus.

Cardiorespiratory functions were normal. The serum creatine kinase (CK) level was 495 IU/l (normal range 51–197 IU/l). Muscle CT scans revealed generalized volume loss, especially in the hamstrings, and areas of low density in the paraspinal muscles (Fig. 1). Needle electromyogram showed mixed neurogenic and myogenic patterns in biceps brachii and tibialis anterior muscles. Nerve conduction velocities of the median and tibialis posterior nerves were normal. No mutations were found in the SMN gene for spinal muscular atrophy; FSHD was ruled out by Southern blot.

The proband's mother is 35 years old. She developed foot-drop on the left at age 29 and became wheelchair-bound 5 years after the onset. Her father is Spanish and her mother is of Filipino and Chinese descent. Clinical examination revealed moderate generalized muscle atrophy and weakness. She was able to sit without support. She could raise her right arm up to the horizontal, but she was unable to raise her legs and left upper limb, against gravity. The spine was not rigid. Deep tendon reflexes were hypoactive. Facial and extra-ocular muscles were spared. The remainder of the physical examination was normal. Serum CK was slightly increased to 477 IU/l.

2.2. Muscle pathology

Muscle biopsy was performed on the left biceps brachii in the proband at age 11. His mother had two biopsies: left biceps brachii muscle and the left quadriceps femoris muscle at age 31. Biopsy specimens were frozen in isopentane cooled in liquid nitrogen. Serial 10 μm cryostat sections were stained with various histochemical methods. For electron microscopy, the muscle specimens were fixed in 2.5% glutaraldehyde in 0.1 M cacodylate buffer; ultrathin sections were double stained with uranyl acetate and lead citrate.

In the proband, there were clusters of atrophic fibers of 5–25 μm in diameter in a few fascicles (Fig. 2a–f), frequently with enlarged nuclei. Non-atrophic fibers showed moderate variation in fiber size ranging from 60–95 μm in diameter. Only a few fibers had internal nuclei. Endomysial fibrous tissue was increased in the atrophic fascicles. Adipose tissue was not increased. On modified Gomori trichrome (mGT), cytoplasmic bodies were seen in scattered fibers. There were no nemaline bodies, rimmed vacuoles or ragged-red fibers. On ATPase, there was mild fiber type grouping.

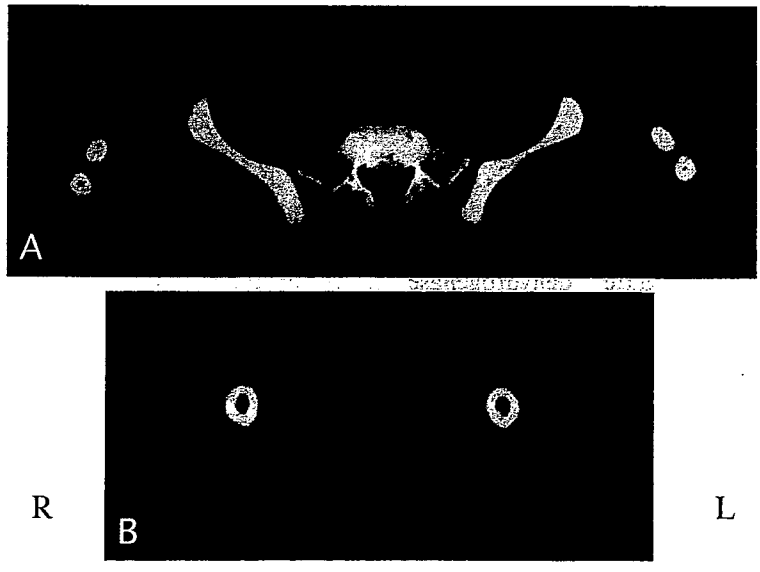

Fig. 1. Muscle computer tomography of the proband. The paraspinal muscles are almost totally replaced by fat tissue (A); the hamstring muscles are atrophic and exhibit moth-eaten appearance (B).

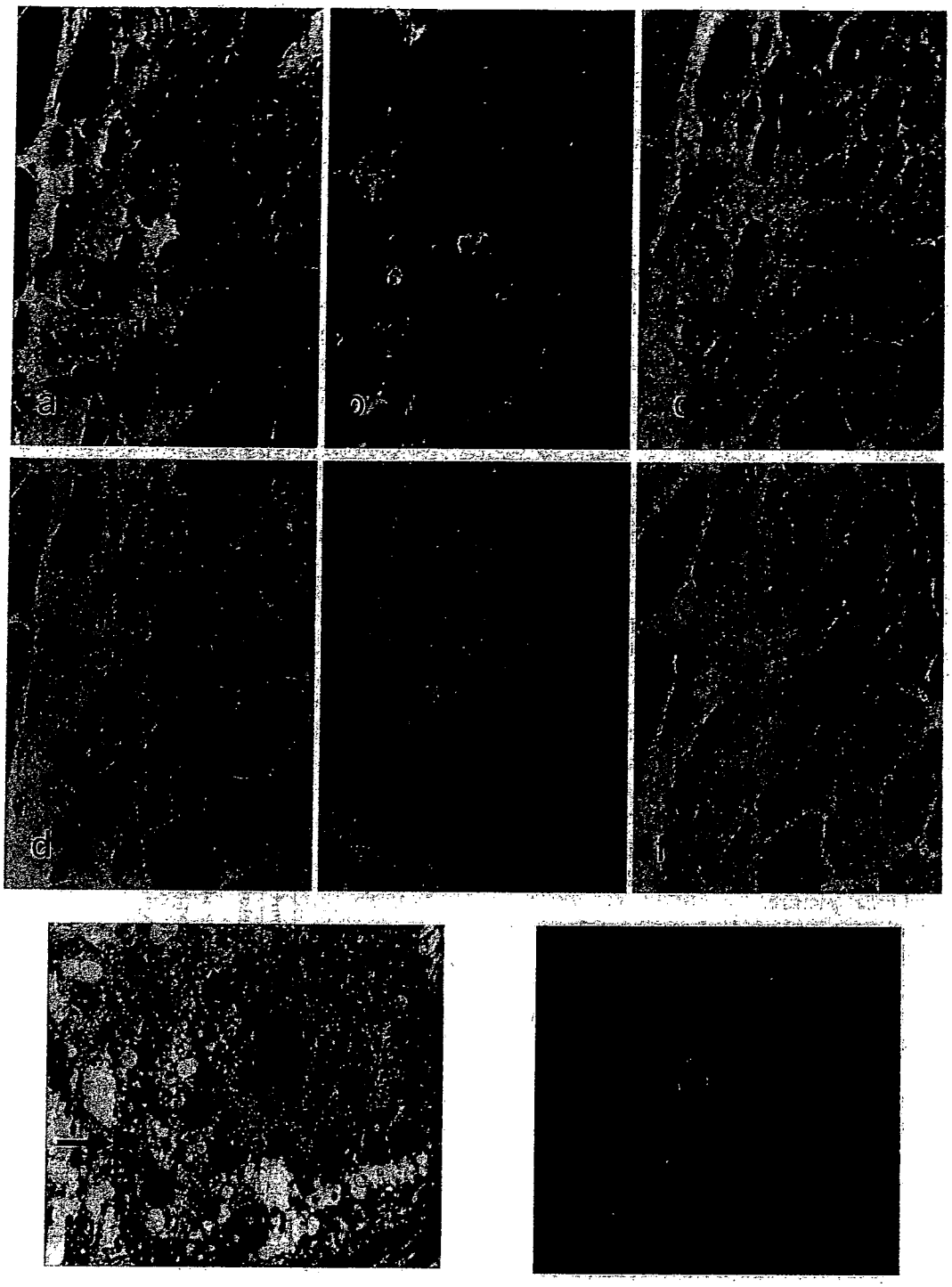

Fig. 2. Serial frozen sections (a–f) and an electron micrograph (g) from patient 1 and representative muscle pathology from patient 2 (h). In hematoxylin and eosin stain, atrophic fibers with reducing bodies are seen to be aggregated, (a). The reducing bodies are eosinophilic (a) and stained dark purple on modified Gomori trichrome (b), strongly reactive to NADH-TR (c), have increased enzymatic activity in acid phosphatase (d), and negative for periodic acid Schiff (PAS) staining suggesting that there is no glycogen component (e). They are strongly stained with MAG (f) showing "reducing activity" to nitroblue tetrazolium. Arrows in a–f indicate the same fiber with reducing bodies in serial sections. An electron micrograph of the reducing bodies (arrow) surrounding a degenerating nucleus (arrow head) suggesting a close relationship between nuclear change and inclusion body formation (g). In the proband's mother's muscle biopsy (h), there are fibers containing eosinophilic reducing bodies (arrow).

The most striking finding was the presence of reducing bodies in the atrophic fibers which were positively stained with both menadione-linked α-glycerophosphate dehydrogenase (MAG) and MAG without the substrate menadione. They were stained brilliant red with hematoxylin and eosin, dark purple with modified Gomori

trichrome, and dark blue with NADH-tetrazolium reductase.

On electron microscopy, these reducing bodies consisted of clusters of granular material with the same electron density as chromatin granules (Fig. 2g). They frequently encircled both normal-looking and degenerated myonuclei.

In the proband's mother, the overall pathological changes were similar although more fascicles were involved and contained very abundant reducing bodies (Fig. 2h). The inclusions were predominantly seen in type 1 fibers.

3. Discussion

Brooke and Neville were the first to describe two girls with congenital myopathy who had progressive and fatal courses [1] whose muscle biopsies were characterized by the presence of intracytoplasmic inclusion bodies. Since these inclusions reduce nitro-blue-tetrazolium (NBT) without a substrate in the α-glycerophosphate dehydrogenase reaction, the term "reducing body" was coined. Thereafter, many patients with reducing bodies in muscle biopsy have been reported as "reducing body myopathy" [2–10]. The onset of the disease varied from early childhood to adulthood, with different clinical symptoms; some had rapidly progressive and fatal course [1,6] and others showed a relatively benign course [2,5,9]. Initially, RBM was thought to be one of the congenital myopathies, although there is no characteristic clinical picture.

Although both our patients had proximal dominant muscle weakness and tibial muscle involvement other features varied: the onset of the disease was different, only the proband had rigid spine, and his mother's progression was quite rapid. Histopathologically, in both patients, some fascicles were preferentially affected. Inclusion bodies were seen mainly in the atrophic fibers.

There have been four families with RBM including the present family (Table 1) [2,7,10]. The modes of inheritance seem to be different from family to family: probable autosomal dominant or X-linked recessive inheritance in this family and in previous reports [7,8]. Hubner's family probably had an autosomal recessive inheritance. In familial RBM, many patients noticed their symptoms during school age, as in our proband; however, one patient developed weakness of the legs and hands after age 50 [10]. Rigid spine seems to be common in familial patients [7,10], but is not necessarily an initial sign and neither is it pathognomonic. Most patients had predominantly proximal muscle weakness and had no facial muscle involvement or pseudohypertrophy. Furthermore, serum CK was usually normal or only mildly elevated. However, there are no definite differences in clinical features between familial and spo-

Table 1
Previous reports of familial reducing body myopathy

Case	Sex	Onset age	Muscle weakness	Other symptoms	CK	Clinical course	Pathological findings	RB
Hubner et al. [2]	F	11	+	Respiratory insufficiency		27y: bed-ridden	Fibrosis	+
Sister	F	9	+	Respiratory insufficiency		15y: alive	Fibrosis	+
Reichmann et al. [7]	M	6	Proximal dominant	Rigid spine kyphosis	343	42y: wheelchair-bound, dead	Variation in fiber size fibrosis	+
Daughter	F	?	None	Rigid spine kyphosis				
Goebel et al. [10]	M	7	Proximal dominant	Rigid spine	174	8y: wheelchair-bound	Variation in fiber size	Many
Grand mother	F	50	Lower limbs dominant			70y: walk slowly	Small groups of atrophic fibers	+
Patient 1	M	10	Proximal dominant	Rigid spine	495	11y: unable to stand up without support	Focal atrophy	In atrophic fibers
Patient 2 (mother)	F	29	Proximal dominant		477	34y: wheelchair- bound	Focal atrophy	Mainly in atrophic fibers

CK: creatine kinase, RB: reducing body; ?: unknown.

radic patients. Pathologically, Goebel et al. [10] also reported that muscle fascicles with numerous inclusion bodies were adjacent to completely normal fascicles, and such focal degeneration seems to be a characteristic feature of this disorder [6]. It is still uncertain whether familial cases of RBM share a common pathogenetic mechanism with that in sporadic RBM.

Histopathologically there was fiber type grouping in our proband, suggesting a neurogenic process as well. Although needle electromyogram of the right tibialis anterior muscle showed a few giant spikes, careful clinical examination and peripheral nerve conduction studies showed no neurogenic changes. A prominent finding in RBM is that the atrophic fibers with reducing bodies are frequently aggregated in some fascicles, sparing the rest of the fascicle [6,10]. With disease progression, the changes extend diffusely and consequently fibrotic tissue proliferation ensues [6]. This selectivity of fascicular involvement may differ from muscle to muscle, reflecting different degrees and clinical variability.

The origin and significance of the reducing bodies remain unknown. Since these inclusions are usually present around and in the vicinity of myonuclei, association with nuclear changes appears possible, more so since these bodies have the same electron density as that of chromatin granules. By immunohistochemical staining, however, these bodies have no nuclear component.

Acknowledgements

We thank Ms Fumie Uematsu for taking electron micrographs on muscle biopsies. The authors thank Dr. May Christine V. Malicdan for her critical comments on the manuscript. This work is supported in part by the "Research on Health Sciences focusing on Drug Innovation" and the "Research on Psychiatric and Neurological Diseases and Mental Health" from the Japanese Health Sciences Foundation; in part by the "Grant-in-Aid for Scientific Research" from the Japan Society for the Promotion of Science; and in part by the "Research Grant (17A-10) for Nervous and Mental Disorders" from the Ministry of Health, Labour and Welfare.

References

[1] Brooke MH, Neville HE. Reducing body myopathy. Neurology 1972;22:829–40.
[2] Hübner G, Pongratz D. Reducing body myopathy - ultrastructure and classification (author's transl). Virchows Arch A Pathol Anat Histol 1981;392:97–104.
[3] Oh SJ, Meyers GJ, Wilson Jr ER, Alexander CB. A benign form of reducing body myopathy. Muscle Nerve 1983;6:278–82.
[4] Carpenter S, Karpati G, Holland P. New observations in reducing body myopathy. Neurology 1985;35:818–27.
[5] Bertini E, Salviati G, Apollo F, Ricci E, Servidei S, Broccolini A, et al. Reducing body myopathy and desmin storage in skeletal muscle: morphological and biochemical findings. Acta Neuropathol (Berl) 1994;87:106–12.
[6] Kiyomoto BH, Murakami N, Kobayashi Y, Nihei K, Tanaka T, Takeshita K, et al. Fatal reducing body myopathy. Ultrastructural and immunohistochemical observations. J Neurol Sci 1995;128:58–65.
[7] Reichmann H, Goebel HH, Schneider C, Toyka KV. Familial mixed congenital myopathy with rigid spine phenotype. Muscle Nerve 1997;20:411–7.
[8] Goebel HH. Congenital myopathies with inclusion bodies : a brief review. Neuromuscul Disord 1998;8:162–8.
[9] Figarella-Branger D, Putzu GA, Bouvier-Labit C, Pouget J, Chateau D, Fardeau M, et al. Adult onset reducing body myopathy. Neuromuscul Disord 1999;9:580–6.
[10] Goebel HH, Halbig LE, Goldfarb L, Schober R, Albani M, Neuen-Jacob E, et al. Reducing body myopathy with cytoplasmic bodies and rigid spine syndrome : a mixed congenital myopathy. Neuropediatrics 2001;32:196–205.

J. Biochem. 143, 377–383 (2008)
doi:10.1093/jb/mvm230

Quantitative Analysis of CUG-BP1 Binding to RNA Repeats

Daisuke Mori[1,*], Noboru Sasagawa[1,2,*], Yoshihiro Kino[1,3] and Shoichi Ishiura[1,*]

[1]Department of Life Sciences; [2]Center for Structuring Life Sciences, Graduate School of Arts and Sciences, the University of Tokyo, 3-8-1 Komaba, Meguro-ku, Tokyo 153-8902; and [3]Laboratory for Structural Neuropathology, RIKEN-Brain Science Institute, 2-1 Hirosawa, Wako-shi, Saitama 351-0198, Japan

Received November 12, 2007; accepted November 15, 2007; published online November 26, 2007

CUG-binding protein 1 (CUG-BP1) is a member of the CUG-BP1 and ETR-3-like factors (CELF) family of RNA-binding proteins, and is involved in myotonic dystrophy type 1 (DM1). Several mRNA targets of CUG-BP1 have been identified, including the insulin receptor, muscle chloride channel, and cardiac troponin T. On the other hand, CUG-BP1 has only a weak affinity for CUG repeats. We conducted quantitative-binding assays to assess CUG-BP1 affinities for several repeat RNAs by surface plasmon resonance (SPR). Although we detected interactions between CUG-BP1 and CUG repeats, other UG-rich sequences actually showed stronger interactions. Binding constants of CUG-BP1 for RNAs indicated that the affinity for UG repeats was far stronger than for CUG repeats. We also found that N-terminal deletion mutant of CUG-BP1 has UG repeat-binding activity in a yeast three-hybrid system, although C-terminal deletion mutant does not. Our data indicates that CUG-BP1 specifically recognized UG repeats, probably through cooperative binding of RNA recognition motifs at both ends of the protein. This is the first report of a binding constant for CUG-BP1 calculated in vitro.

Key words: binding constant, CUG-BP1, myotonic dystrophy, surface plasmon resonance, triplet-repeat.

Abbreviations: 3-AT, 3-amino triazole; CELF, CUG-BP and ETR3-like factor; DM, myotonic dystrophy; DMPK, DM protein kinase; RRM, RNA recognition motif.

CUG-BP and ETR3-like factor (CELF) proteins, also known as Bruno-like (BRUNOL) proteins, are a family of highly conserved RNA-binding proteins (1, 2). All mammalian CELF proteins contain three RNA recognition motifs (RRMs; also referred to as RNP domains or consensus RNA-binding domains) and have a similar organization: two closely spaced N-terminal RRMs, a divergent hinge region of 60–90 residues, and a C-terminal RRM (1). RRM-containing proteins represent the largest family of RNA-binding proteins and perform various functions in post-transcriptional gene regulation. CUG-binding protein 1 (CUG-BP1) was the first discovered member of the CELF proteins and acts as a regulator of alternative splicing (1, 3–5), translation (6, 7) and deadenylation (8, 9).

Several reports have shown the involvement of this protein in myotonic dystrophy (dystrophia myotonica or DM) type 1 (DM1) (3–6, 10 and 11 for review). As indicated by its name, the binding of CUG-BP1 to expanded CUG repeats was first demonstrated in the onset of DM (12, 13). Indeed, CUG-BP1 was first identified as a protein binding to a $(CUG)_8$ probe in a gel retardation assay (12, 13). However, whether this protein does actually bind expanded repeats is controversial. For example, it does not specifically co-localize with nuclear RNA foci, formed by expanded repeats in DM1 cells (14). Moreover, contrary to its name, CUG-BP1 actually appears to specifically bind to UG motifs, rather than to CUG repeats, in a yeast three-hybrid system (15, 16).

Muscleblind-like proteins, another group of RNA-binding proteins, have recently emerged as more plausible proteins for the sequestration model (14, 16). Nevertheless, CUG-BP1 is still an important factor in DM1, because reports have shown up-regulation of CUG-BP1 protein levels in DM1 cells by still unknown mechanisms, and its elevated activity is thought to cause abnormalities in DM1 (4).

CUG-BP1 may contribute to the aberrant splicing of multiple genes, a hallmark of DM1. Alternative splicing of the insulin receptor (IR), muscle chloride channel (CLCN1), cardiac troponin T (cTNT) and other genes is regulated by CUG-BP1, and the splicing patterns of these genes are altered in DM1 patients (3–5, 17).

In addition to splicing defects, it has also been suggested that CUG-BP1 is involved in the altered translation of p21 and MEF2A in DM1 cells, and leads to defects in myogenic progression (6). Furthermore, over-expression of CUG-BP1 in mice recapitulated some abnormalities similar to those observed in DM1 patients, such as aberrant splicing and histological impairment of the muscle (10). It is also described that mice over-expressing normal DMPK 3′-untranslated region had increased levels of CUG-BP1 in skeletal muscle, as seen in individuals with DM1 (18). Thus, understanding CUG-BP function and its target genes is important for an understanding of DM pathogenesis.

*The first two authors contributed equally to this work.
*To whom correspondence should be addressed. Tel/Fax: +81-3-5454-6739, E-mail: cishiura@mail.ecc.u-tokyo.ac.jp.

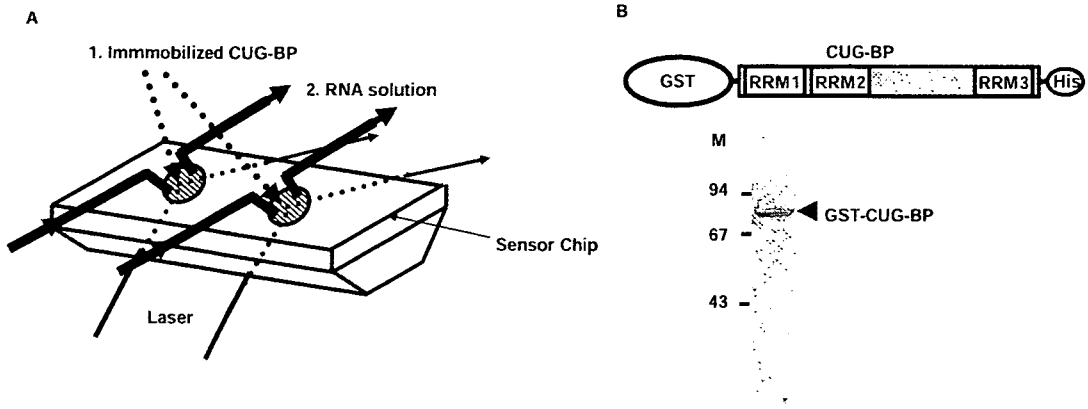

Fig. 1. Design of SPR experiment and purified protein used in this study. A: Schematic illustration of the SPR analysis. First, purified CUG-BP1 was immobilized on the gold layer of the sensor chip. RNA solution flowed through the sensor chip surface. CUG-BP1-RNA interactions were detected as the difference in resonance angle of the surface plasmon, elicited by a laser. B: Recombinant CUG-BP1. (Top) Structure of recombinant CUG-BP1. CUG-BP1 was fused with glutathione S-transferase at the N-terminus and a 6• His-tag at the C-terminus. (Bottom) Purified GST-CUG-BP1 used in this study. The purified fraction was subjected to SDS-PAGE and stained with Coomassie Brilliant Blue. Molecular weight is indicated by M.

Despite its importance, the RNA-binding specificity of CUG-BP1 remains to be determined, primarily because of the lack of biochemical analysis directly addressing the binding constants. In this article, we conducted an in vitro binding analysis between CUG-BP1 and CUG and other repetitive nucleotides to examine whether CUG-BP1 could interact with CUG repeats and to find specific target sequences of CUG-BP1.

MATERIALS AND METHODS

Synthesis of DNAs Containing Repetitive Sequences—DNA fragments of repetitive sequences such as $(CUG)_{140}$, $(UG)_{24}$, $(UG)_{41}$ and $(UAUG)_{14}$, were synthesized by a non-template polymerase chain reaction (PCR) method with Pfu Turbo polymerase (Stratagene) through 5–25 cycles of amplification (968C for 1 min, 608C for 30 s and 728C for 90 s) after 10 rounds of 968C for 1 min, 608C for 30 s and 728C for 1 min (19). DNAs for other short repeat fragments were purchased from Proligo, Japan.

In vitro Transcription—DNA fragments with repetitive sequences were ligated into the HincII site of a pBluescriptII SK(+)-derived vector containing an ApaI–Eco52I site deletion and a HincII site insertion. Using DNA fragments from these constructs as templates, RNAs were transcribed with the MEGAscript T7 or T3 kits (Ambion) in a 20 mL reaction. The quantity of the synthesized mRNAs was checked by the absorbance at 260 and 280 nm. Their quality was checked by denaturing agarose gel electrophoresis.

SPR Biosensor Analysis—In the SPR biosensor analysis, using SPR-MACS (Moritex), the sensor chip was coated with 4,4'-dithiodibuthyric acid (DDA), 1-ethyl-3-(3-dimethylaminopropyl) carbodiimide (EDC) and N-hydroxysuccinimide (NHS), according to the manufacturer's protocol. CUG-BP1 was immobilized on the sensor chip by amino-coupling, and RNAs were passed over the protein surface (Fig. 1A). The binding reaction was performed in a running buffer of 10 mM HEPES (pH 8.0), 150 mM NaCl, 1 mM dithiothreitol (DTT), at a flow rate of 10 ml/min. Association and dissociation were measured in arbitrary units and displayed on a graph (sensorgram). The RNAs binding to the protein surface were released with 9 mM NaOH as a regeneration solution (Fig. 2). After this treatment, the next binding experiment was performed. Binding constants were calculated based on the sensorgram using Method 2 software (Moritex).

Bacterial Expression and Purification of Recombinant Double-Tagged CUG-BP1 and Mutants—An expression vector, human CUG-BP1 in pET-GX, has been previously described (16). BL21(DE3) competent cells (Stratagene) were transformed with this construct and used for protein expression. A single colony was grown overnight at 378C in LB medium with 50 mg/ml ampicillin, diluted 1:20 in fresh medium, and then grown at 378C until A_{600} reached 0.25–0.30. IPTG was then added to the culture to a final concentration of 0.1 mM and incubated for a further hour at 378C. The cells were harvested as a pellet and were resuspended in 30 ml PBS containing 1/500 volume of proteinase inhibitor mixture (Wako), 1 mM PMSF and 1 mM DTT, and were lysed in a French press (Ohtake Works, Co.). The total cell lysate was centrifuged (15 min, 15,000 g). The supernatant was subjected to affinity purification using GSTrap FF affinity columns (Amersham Pharmacia Biotech) with an FPLC system and 300 ml (bed volume) of BD Talon affinity resin (Clontech), according to the manufacturer's protocol. The protein sample was dialysed twice against HBS buffer (10 mM HEPES-NaOH pH 8.0, 150 mM NaCl, 1 mM DTT). The quantity and purity were checked on SDS-polyacrylamide electrophoresis gels, stained with Coomassie brilliant blue (CBB; Fig. 1B).

Yeast Three-Hybrid System—To make CUG-BP1 RRM mutants, conserved residues were changed by site-directed mutagenesis, K59Q and F63A in Mut1; R148Q and F152A in Mut2 and K438Q and F442A in Mut3.

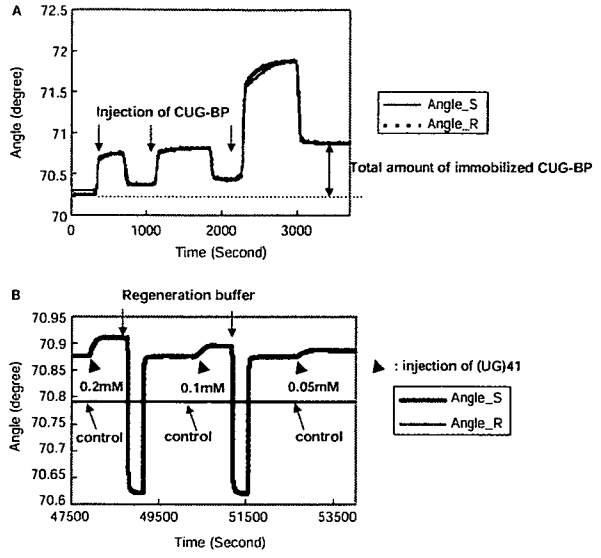

Fig. 2. SPR measurement. A: Immobilization of CUG-BP1. The signals of the resonance angle were monitored during the injection and immobilization of purified CUG-BP1 protein on the gold layer. Angle S and Angle R indicate the resonance angles at the measurement spots for the sample and the reference control, respectively. Arrows indicate the time when CUG-BP1 solution was injected. Multiple injections enhanced the amount of immobilized CUG-BP1. B: An example of SPR measurement of CUG-BP1 and $(UG)_{41}$ repeat. Arrows show the time point when $(UG)_{41}$ RNA solution at the concentration indicated was injected. Each time after measurement, regeneration buffer was injected to wash off RNAs bound to CUG-BP1. Injection of a higher concentration of $(UG)_{41}$ resulted in more rapid and larger changes in the signals.

Mut(1 + 2), Mut(2 + 3) and Mut(1 + 3) contained two combined RRM mutations. To make deletion mutants, fragments of CUG-BP1 (Fig. 4), were amplified by PCR. • RRM1, • RRM2, • RRM3 and • linker constructs have been described previously (15). In the HIS3 assay, yeast strain L40-coat was transformed with pGAD and pIIIA/MS2-2 vectors encoding CUG-BP1 mutants and RNAs, respectively, and selected on plates lacking leucine and uracil. Yeast transformants were picked and spotted onto selection plates lacking leucine, uracil and histidine, with or without 0.5, 1, 2.5, 5 or 10 mM 3-amino triazole (3-AT) (16). The plates were incubated at 308C for about 1 week and the viability of the yeast transformants was analysed. We classified the binding activity as (+++++), (++++), (+++), (++) and (+) when yeast growth was observed on the plates containing 10, 5, 2.5, 1 and 0.5 mM 3-AT, respectively; no growth of yeast transformants with empty vectors was observed on 0.5 mM 3-AT plates.

RESULTS

SPR Analysis—We used a recombinant CUG-BP1 protein, fused with glutathione S-transferase (GST) at the N-terminus and a histidine tag at the C-terminus of the protein (Fig. 1B). For measurements, CUG-BP1 was immobilized on the sensor chip and then RNA solution was passed over the chip (Fig. 1A). By detecting changes in the sensorgram, we could confirm the immobilization of CUG-BP1 (Fig. 2A) and the binding of RNAs to CUG-BP1 (an example is shown in Fig. 2B).

Comparative Analysis of CUG-BP1's RNA-Binding in an SPR Assay—First, we determined whether CUG-BP1 could bind to the $(CUG)_8$ or $(CUG)_{140}$ repeats. We detected weak binding of CUG-BP1 to $(CUG)_8$ and $(CUG)_{140}$ repeats, with K_d values of 27.2 mM and 6 mM, respectively, but detected no binding of CUG-BP1 to a $(CAG)_{10}$ repeat (Fig. 3, Table 1).

Next, we compared UG repeat sequences to CUG repeats, because the former interacted with CUG-BP1 in previous yeast three-hybrid experiments (15,16). We detected stronger binding of CUG-BP1 to UG repeats than to CUG repeats (Fig. 3, Table 1). Thus, CUG-BP1 actually bound tighter to a UG motif than to a CUG motif.

UG Dinucleotide is a Preferred Binding Motif of CUG-BP1—We next asked which was more important for the binding of CUG-BP1, the content of 'U' and 'G' nucleotides in the RNA sequence or that of 'UG' dinucleotides. Although $(UG)_{15}$ and $(UUGG)_7$ contain 15 Us and 15 Gs (Table 2), the binding of CUG-BP1 to $(UUGG)_7$ was weaker than to $(UG)_{15}$. Remarkably, another RNA $(UUUGGG)_5$, which has the same number of Us and Gs as $(UG)_{15}$ and $(UUGG)_7$, showed no detectable binding to CUG-BP1. These results suggest that the content of the UG dinucleotide motif, but not the number of U and G nucleotides, is important for recognition by CUG-BP1.

CUG-BP1 can bind to an RNA sequence, named embryonic deadenylation element (EDEN), which is composed of repetitive UAUG motifs (20). Thus, UA may be another recognition motif for CUG-BP1. To test this, we examined $(UAUG)_7$ as a probe. Compared to $(UG)_{15}$, $(UAUG)_7$ showed decreased binding to CUG-BP1, implying a weaker affinity for the UA motif than for a UG motif. Consistently, one substitution of U to A in one of the middle UG motifs in $(UG)_{15}$ (UG15mut, Table 2) doubled the value of K_d. Thus, UA is not as preferred a binding motif for CUG-BP1 as UG. Furthermore, we could detect no binding to a pure UA repeat, $(UA)_{15}$. This may reflect intramolecular or intermolecular base-pairing between UA repeats, which may affect the binding of CUG-BP1.

Finally, we examined the binding of CUG-BP1 to UGG (GUG/GGU) and UUG (UGU/GUU) motifs, because both GUG and UGU motifs can be found in a UG dinucleotide repeat. Also, repeats of both UGG/GUG/GGU and UUG/UGU/GUU motifs contain UG motifs. In both $(UGG)_{10}$ and $(UUG)_{10}$, the number of non-overlapping UG motifs was smaller than that of $(UG)_{15}$, while the number of GUG and UGU motifs, respectively, was larger than in $(UG)_{15}$. This comparison enabled the determination of whether the GUG or UGU motifs were more preferred than UG. Both $(UGG)_{10}$ and $(UUG)_{10}$ showed lower affinities than $(UG)_{15}$ (Table 2). From these results, we conclude that CUG-BP1 recognizes a UG (or GU) dinucleotide repeat as a binding motif, rather than other UG-rich repeats.

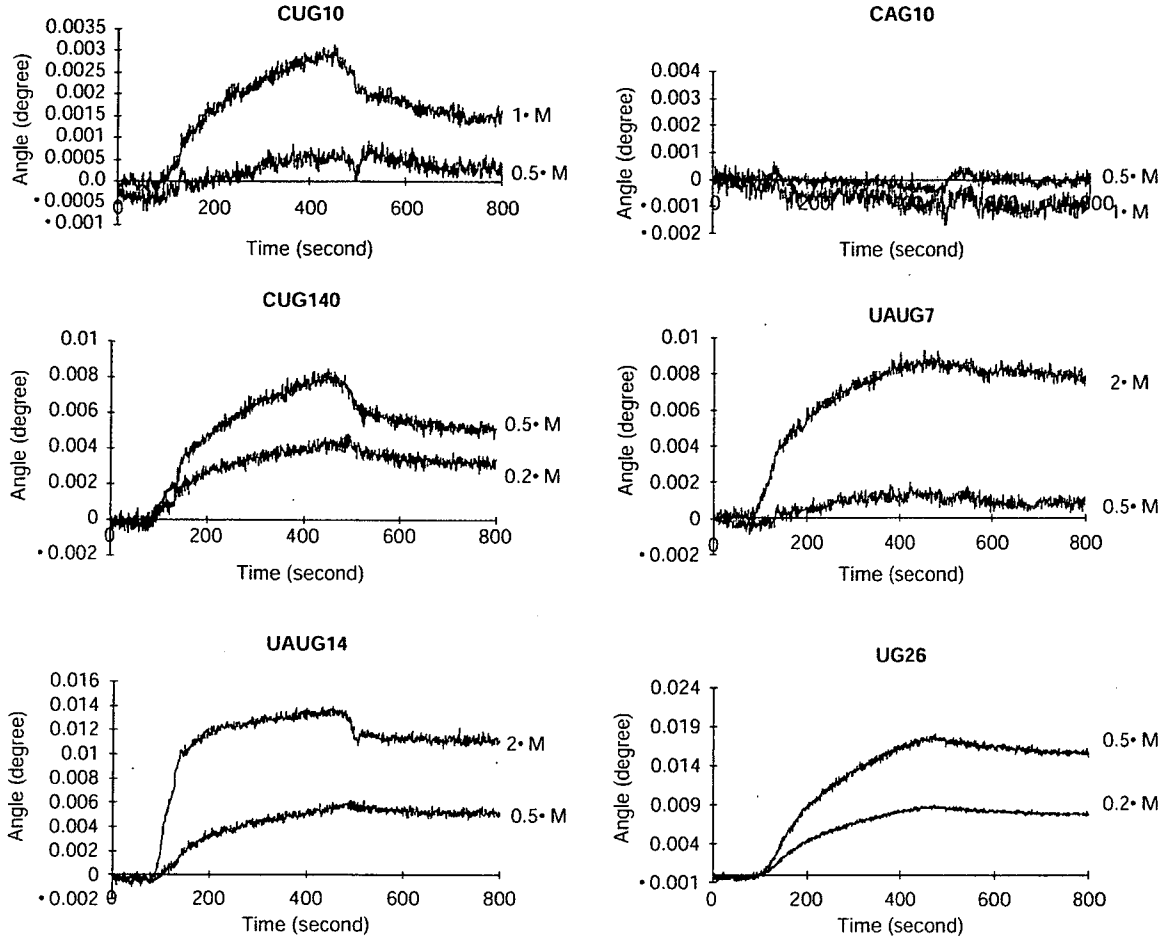

Fig. 3. Binding of various repetitive RNAs in the SPR analysis. SPR signals obtained with repetitive RNAs were monitored. Each RNA sequence is indicated above the panel. Concentrations (mM) represent that of injected RNA.

Table 1. Binding constants of CUG-BP with di-, tri- and tetra-nucleotide repeats.

Repeat	K_d (mM)	k_{ass} ($M^{-1}s^{-1}$)	k_{diss} (s^{-1})
(CA)15	–	–	–
(CAG)10	–	–	–
(CUG)10	27• 12	$4.6• 2.5• 10^2$	$6.6• 0.3• 10^{-3}$
(CUG)140	6.0• 2.0	$2.1• 1.3• 10^3$	$9.2• 0.9• 10^{-3}$
(UAUG)7	1.3• 0.1	$2.1• 0.2• 10^3$	$2.6• 0.2• 10^{-3}$
(UAUG)14	1.3• 0.3	$2.6• 0.3• 10^3$	$3.4• 1.1• 10^{-3}$
(UG)15	0.25• 0.10	$9.0• 1.0• 10^3$	$2.3• 1.1• 10^{-3}$
(UG)26	0.12• 0.05	$9.6• 1.7• 10^3$	$1.1• 0.03• 10^{-3}$
(UG)41	0.06• 0.02	$3.1• 0.7• 10^4$	$1.9• 0.7• 10^{-3}$

N=3, mean• SE.

$(UGG)_{10}$ and $(UUG)_{10}$ showed similar binding to CUG-BP1, while $(CUG)_{10}$, which contains the same number of UG motifs, showed a 7-fold increased K_d value. This apparently suggests that CUG is not an optimal binding motif for CUG-BP1, despite its name.

Mutation Analysis of CUG-BP1 in a Yeast Three-Hybrid System—Although CUG-BP1 has three RRM RNA-binding domains, it is still unknown which RRM is responsible for binding to a UG repeat. Previously, we reported that these three RRMs redundantly contributed to binding to a UG repeat (15). To determine the RNA-binding domain of CUG-BP1 more specifically, we conducted a yeast three-hybrid assay using several RRM mutants, in which two conserved residues in the respective RRM were disrupted. Mutation of one of any RRMs reduced binding of CUG-BP1 to UG repeats (Fig. 4). Double mutants did not have substantial-binding ability. On the other hand, the results of deletion mutants indicated that the C-terminal region of CUG-BP1 has an important function to bind to UG repeats. N1 and N2 (or N3) mutants did not show ability to bind to UG repeats. In contrast, a deletion mutant of both RRM1 and RRM2 (C2) still showed binding to a UG repeat. In addition, the experiment showed that a small portion of CUG-BP1 linker region was also essential for efficient binding to UG repeats.

Table 2. K_d values of CUG-BP with di-, tri- and tetra-nucleotide repeats (30 nt.).

Repeat	Sequence (30 nt)	K_d (mM)
(UG)15	UGUGUGUGUGUGUGUGUGUGUGUGUGUG	0.25 • 0.1
(UG)15mut	UGUGUGUGUGUGUAUGUGUGUGUGUGUG	0.52 • 0.05
(UAUG)7	UAUGUAUGUAUGUAUGUAUGUAUGUAUGUA	1.3 • 0.1
(UUGG)7	GUUGGUUGGUUGGUUGGUUGGUUGGUUGGU	3.3 • 0.4
(UUUGGG)5	UUUGGGUUUGGGUUUGGGUUUGGGUUUGGG	–
(UA)15	UAUAUAUAUAUAUAUAUAUAUAUAUAUAUA	–
(UGG)10	UGGUGGUGGUGGUGGUGGUGGUGGUGGUGG	4.1 • 0.6
(UUG)10	UUGUUGUUGUUGUUGUUGUUGUUGUUGUUG	3.6 • 0.1
(CUG)10	CUGCUGCUGCUGCUGCUGCUGCUGCUGCUG	27.2 • 12
(CAG)10	CAGCAGCAGCAGCAGCAGCAGCAGCAGCAG	–

N = 3, mean • SE. (UG)15mut has UA in the seventh UG repeat (underlined).

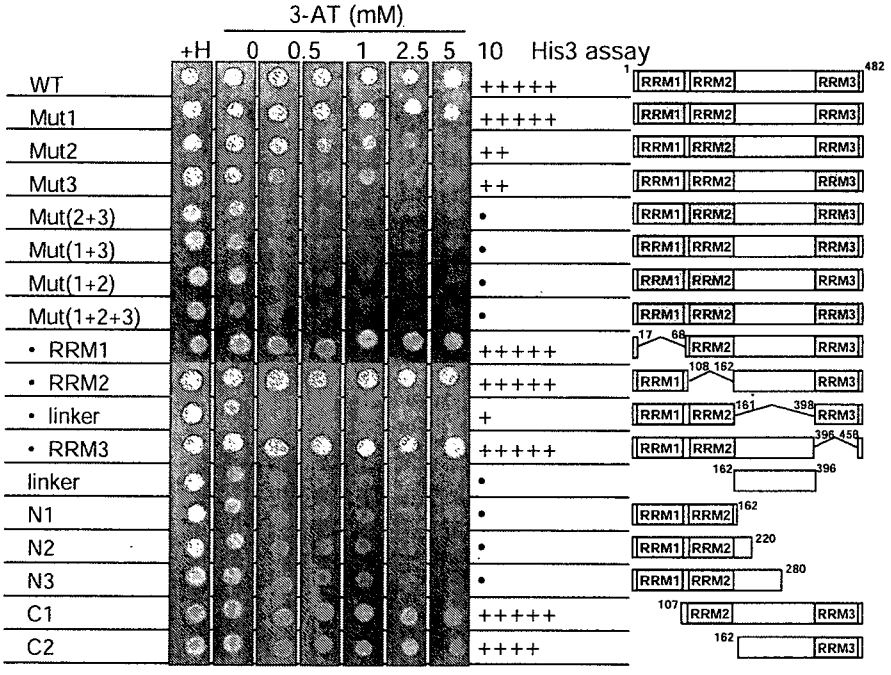

Fig. 4. Yeast three-hybrid analysis of CUG-BP1 mutants. Structures of CUG-BP1 mutants used in the assay are shown on the right. Mutated RRM motifs are indicated by hatched boxes. Results of the yeast three-hybrid HIS3 assay are shown in the middle. Wild-type or mutant CUG-BP1 constructs and the $(UG)_{24}$ expression vector were transformed into yeast cells. Transformants were seeded to test their viability on the selection plates, lacking histidine but containing 0.5, 1, 2.5, 5 or 10 mM 3-amino triazole (3-AT), a competitive inhibitor of histidine synthesis. Viability of yeast transformants was classified as follows: +++++, ++++, +++, ++, + means, viable with 10, 5, 2.5, 1 and 0.5 mM 3-AT, respectively and – means, not viable with 0.5 mM 3-AT.

DISCUSSION

CUG-BP1 Specifically Binds to (UG) Dinucleotide Repeat RNA in an SPR Assay—We previously reported that CUG-BP1 preferentially bound to UG dinucleotides in a yeast three-hybrid assay (15). In the current report, we used a SPR assay to determine actual binding constants of CUG-BP1 with RNAs in vitro. In the SPR assay, CUG-BP1 bound to $(CUG)_8$ and $(CUG)_{140}$ repeats, but not to a $(CAG)_{10}$ repeat. However, the dissociation constants obtained in our experiments between CUG-BP1 and $(CUG)_{10}$ or $(CUG)_{140}$ suggested that CUG-BP1 does not bind very strongly to the CUG triplet repeat in vitro or possibly under physiological conditions. The moderate binding between CUG-BP1 and CUG repeats in addition to differences in experimental systems may explain some of the previous controversial results.

In contrast to binding to the CUG repeat, CUG-BP1 bound strongly to UG dinucleotide repeats in the SPR assay. Subsequently, a comparative analysis using UG-like repetitive sequences (Table 2) revealed that CUG-BP1 prefers 'pure' UG dinucleotide repeats as binding targets, rather than other UG-rich sequences, such as $(UAUG)_7$ or $(UUG)_{10}$. Because longer UG repeats seemed to bind more strongly to CUG-BP1 (Table 1) and pure UG repeat tracts were sufficient for binding to CUG-BP1, we conclude that CUG-BP1 recognizes UG repeats as a

binding target. Importantly, a recent report showed that ETR-3, the closest CELF protein to CUG-BP1, recognized UG repeats as well as UGUU, which were identified from systematic evolution of ligands by exponential enrichment (SELEX) (21). These results suggest that these two CELF proteins have similar binding specificities. However, UGUU motifs were included in the $(UUG)_{10}$ repeat used in our study; binding was not as strong as to $(UG)_{15}$ in the assays. Thus, CUG-BP1 may bind more specifically to UG motifs than UGUU motifs. However, we cannot exclude that efficient recognition of UGUU motifs by CUG-BP1 requires a particular spacing of nucleotides between the UGUU motifs.

The Importance of RRMs in the Binding to UG Repeats—In our previous study, we examined the binding affinities of CUG-BP1 deletion mutants in a yeast three-hybrid assay and showed that no complete loss of RNA-binding ability of CUG-BP1 occurred when any of the three RRMs was singly deleted (15). This suggests redundant RNA recognition among the RRMs. We attempted to reveal more detail about the structural requirements of the RNA-binding abilities of CUG-BP1 using additional mutant proteins.

Deletion analyses indicated that the N-terminal fragment (containing RRM1 and RRM2) did not show ability to bind to UG repeats, although Mut3 had binding affinity to UG repeats. On the contrary, the C-terminal fragment (containing RRM3) of CUG-BP1 harbored UG repeat-binding abilities, although Mut(1 + 2) did not show any binding to UG repeats. These results indicate that a conformational change occurs in deletion mutants, and that a conformational and cooperative interaction of three RRMs is important for CUG-BP1 function.

Moreover, a deletion of linker (• linker) strongly reduced binding affinity to UG repeats. Taken that the linker region itself did not have RNA binding ability into account, this result indicates that the linker region is important for cooperative RNA-binding by both N- and C-terminus, possibly by modulating the conformation of the entire protein. Alternatively, it is conceivable that this linker region modulates the RNA-binding abilities or functions of CUG-BP1 by mediating multimer formation, as reported in a study of EDEN-BP, a CUG-BP1 ortholog in frogs (22).

Biological Implication of UG Binding of CUG-BP1—The characterization of the RNA-binding specificity of a protein is important in understanding its function or physiological role. In general, the presence of multiple binding motifs for an RNA-binding protein would enhance the probability of the protein binding to the RNA. From our results, it is predicted that the number of UG motifs in an RNA stretch will determine the affinity of CUG-BP1 for it. If this is so, the degree of influence on target RNAs of CUG-BP1 would be variable, depending on the content or length of a UG repeat. Indeed, we observed length-dependent binding of CUG-BP1 with UG repeats (Table 1).

Although there are many pure UG repeat-containing genes in the human genome (15), few of them have been analysed as targets of CUG-BP1. It would be of value to focus on such genes to obtain further insight into CUG-BP1 function. Several reports have described functional target sequences of CUG-BP1 (3–5). However, there is no previous example of a pure UG repeat as a functional target of CUG-BP1. Thus, it is of importance to examine the functional interaction between CUG-BP1 and UG-containing genes. Because CUG-BP1 may have pathogenic roles in DM, identification of its target genes may be a beneficial way to understand the molecular mechanism of this disease.

UG-binding ability is apparently a feature of CUG-BP1 (and ETR-3); another RNA-binding protein, TDP-43, also preferentially binds to a UG repeat (23). As TDP-43 is a splicing regulator, like CUG-BP1, there may be some functional connection, such as antagonism, between these proteins that bind to UG repeat-containing RNAs. In addition, functional competition or cooperation between CUG-BP1 and ETR-3 or other CELF proteins, which may share RNA substrates, would be an interesting area of future work toward understanding the importance of UG-binding proteins.

Yeast three-hybrid components were kindly provided by Dr Marvin Wickens. This work was supported in part by grants from the Ministry of Health, Labor and Welfare, Japan (17A-10) and the Ministry of Education, Science, Sports and Culture, Japan.

REFERENCES

1. Ladd, A.N., Charlet, N., and Cooper, T.A. (2001) The CELF family of RNA binding proteins is implicated in cell-specific and developmentally regulated alternative splicing. Mol. Cell. Biol. 21, 1285–1296
2. Good, P.J., Chen, Q., Warner, S.J., and Herring, D.C. (2000) A family of human RNA-binding proteins related to the Drosophila Bruno translational regulator. J. Biol. Chem. 275, 28583–28592
3. Philips, A.V., Timchenko, L.T., and Cooper, T.A. (1998) Disruption of splicing regulated by a CUG-binding protein in myotonic dystrophy. Science 280, 737–741
4. Savkur, R.S., Philips, A.V., and Cooper, T.A. (2001) Aberrant regulation of insulin receptor alternative splicing is associated with insulin resistance in myotonic dystrophy. Nat. Genet. 29, 40–47
5. Charlet, B.N., Savkur, R.S., Singh, G., Philips, A.V., Grice, E.A., and Cooper, T.A. (2002) Loss of the muscle-specific chloride channel in type 1 myotonic dystrophy due to misregulated alternative splicing. Mol. Cell. 10, 45–53
6. Timchenko, N.A., Iakova, P., Cai, Z.J., Smith, J.R., and Timchenko, L.T. (2001) Molecular basis for impaired muscle differentiation in myotonic dystrophy. Mol. Cell. Biol. 21, 6927–6938
7. Timchenko, N.A., Welm, A.L., Lu, X., and Timchenko, L.T. (1999) CUG repeat binding protein (CUGBP1) interacts with the 5′ region of C/EBPbeta mRNA and regulates translation of C/EBPbeta isoforms. Nucleic Acids Res. 27, 4517–4525
8. Paillard, L., Legagneu, X V., and Osborne, H.B. (2003) A functional deadenylation assay identifies human CUG-BP as a deadenylation factor. Biol. Cell 95, 107–113
9. Moraes, K.C., Wilusz, C.J., and Wilusz, J. (2006) CUG-BP binds to RNA substrates and recruits PARN deadenylase. RNA 12, 1084–1091
10. Ho, T.H., Bundman, D., Armstrong, D.L., and Cooper, T.A. (2005) Transgenic mice expressing CUG-BP1 reproduce splicing mis-regulation observed in myotonic dystrophy. Hum. Mol. Genet. 14, 1539–1547

11. Ranum, L. and Cooper, TA. (2006) RNA-mediated neuromuscular disorders. Annu. Rev. Neurosci. 29, 259–277
12. Timchenko, L.T., Timchenko, N.A., Caskey, C.T., and Roberts, R. (1996) Novel proteins with binding specificity for DNA CTG repeats and RNA CUG repeats: implications for myotonic dystrophy. Hum. Mol. Genet. 5, 115–121
13. Timchenko, L.T., Miller, J.W., Timchenko, N.A., DeVore, D.R., Datar, K.V., Lin, L., Roberts, R., Caskey, C.T., and Swanson, M.S. (1996) Identification of a (CUG)n triplet repeat RNA-binding protein and its expression in myotonic dystrophy. Nucleic Acids Res. 24, 4407–4414
14. Fardaei, M., Rogers, M.T., Thorpe, H.M., Larkin, K., Hamshere, M.G., Harper, P.S., and Brook, J.D. (2002) Three proteins, MBNL, MBLL and MBXL, co-localize in vivo with nuclear foci of expanded-repeat transcripts in DM1 and DM2 cells. Hum. Mol. Genet. 11, 805–814
15. Takahashi, N., Sasagawa, N., Suzuki, K., and Ishiura, S. (2000) The CUG-binding protein binds specifically to UG dinucleotide repeats in a yeast three-hybrid system. Biochem. Biophys. Res. Commun. 277, 518–523
16. Kino, Y., Oma, Y., Sasagawa, N., and Ishiura, S. (2004) Muscleblind protein, MBNL1/EXP, binds specifically to CHHG repeats. Hum. Mol. Genet. 13, 495–507
17. Nezu, Y., Kino, Y., Sasagawa, N., Nishino, I., and Ishiura, S. (2007) Expression of MBNL and CELF mRNA transcripts in muscles with myotonic dystrophy. Neuromuscular Disord. 17, 306–312
18. Mahadevan, M.S., Yadava, R.S., Yu, Q., Balijepalli, S., Frenzel-McCardell, C.D., Bourne, T.D., and Phillips, L.H. (2006) Reversible model of RNA toxicity and cardiac conduction defects in myotonic dystrophy. Nat. Genet. 38, 1066–1070
19. Takahashi, N., Sasagawa, N., Suzuki, K., and Ishiura, S. (1999) Synthesis of long trinucleotide repeats in vitro. Neurosci.Lett. 262, 45–48
20. Paillard, L., Omilli, F., Legagneux, V., Bassez, T., Maniey, D., and Osborne, H. B. (1998) EDEN and EDEN-BP, a cis element and an associated factor that mediate sequence-specific mRNA deadenylation in Xenopus embryos. EMBO J. 17, 278–287
21. Faustino, N.A. and Cooper, T.A. (2005) Identification of putative new splicing targets for ETR-3 using sequences identified by systematic evolution of ligands by exponential enrichment. Mol. Cell Biol. 25, 879–887
22. Bonnet-Corven, S., Audic, Y., Omilli, F., and Osborne, H.B. (2002) An analysis of the sequence requirements of EDEN-BP for specific RNA binding. Nucleic Acids Res. 30, 4667–4674
23. Buratti, E., Dork, T., Zuccato, E., Pagani, F., Romano, M., and Baralle, F.E. (2001) Nuclear factor TDP-43 and SR proteins promote in vitro and in vivo CFTR exon 9 skipping. EMBO J. 20, 1774–1784

Journal of Neuroscience Research 00:000–000 (2008)

MBNL1 Associates With YB-1 in Cytoplasmic Stress Granules

Hayato Onishi,[1] Yoshihiro Kino,[1,2] Tomoko Morita,[1] Eugene Futai,[1] Noboru Sasagawa,[1] and Shoichi Ishiura[1]*

[1]Department of Life Sciences, Graduate School of Arts and Sciences, University of Tokyo, Tokyo, Japan
[2]Laboratory for Structural Neuropathology, Brain Science Institute, RIKEN, Tokyo, Japan

The muscleblind-like (MBNL) protein family is thought to be involved in the molecular mechanism of myotonic dystrophy (DM). Although it has been shown to have splicing activity, a broader function in cellular RNA metabolism has been implicated. In this study, we attempted to find the binding proteins of MBNL1 in order to elucidate its physiological function. First, we performed a GST pull-down assay using GST-MBNL1-6xHis as bait. Several proteins were identified, including YB-1, a multifunctional DNA/RNA-binding protein, and DDX1, a DEAD box RNA helicase. MBNL1 formed an RNP complex with YB-1 and DDX1 in binding assays. YB-1 also showed a weak but significant effect on α-actinin splice site selection. Interestingly, in response to stress, MBNL1 moved to cytoplasmic stress granules, where it colocalized with YB-1, which was previously reported to be a component of stress granules. We found that DDX1 also colocalized with MBNL1 at stress granules. These results provide new insight into the dynamics of MBNL1 in response to stress, and they suggest a role for MBNL1 in mRNA metabolism in the cytoplasm.

Key words: myotonic dystrophy; MBNL1; YB-1; stress granules; splicing

Myotonic dystrophy (dystrophia myotonica; DM) is one of the most common human muscular dystrophies, occurring at a frequency of 1 in 8,000 (Harper, 2001). The clinical features of DM include myotonia, cataracts, insulin resistance, and cognitive dysfunction (Meola et al., 2003). DM is an autosomally inherited disorder that is classified into two types, DM1 and DM2, based on the expansion of tri (CTG)- and tetra (CCTG)-nucleotide repeats in the 3′-UTR of *DMPK* (Brook et al., 1992; Mahadevan et al., 1992; Fu et al., 1993) and intron 1 of *ZNF9* (Liquori et al., 2001), respectively. DM1 and DM2 have similar phenotypes even though they are caused by unrelated mutations (Day et al., 2003). Various hypotheses have been proposed to explain how untranslated mutations can lead to a dominant pathogenic phenotype; however, several lines of evidence support a "gain-of-function" model for expanded RNA repeats. No DMPK mutation except for the repeat expansion has ever been reported, indicating that loss of function of DMPK is not the major cause of DM1. Although mice deficient in DMPK show mild myopathy and abnormalities in cardiac conductance, they do not reproduce other symptoms of DM1 (Jansen et al., 1996; Reddy et al., 1996; Berul et al., 1999). On the other hand, mice expressing expanded CUG repeats inserted in the 3′-UTR of the muscle-specific actin gene developed myotonia and DM-like myopathy (Mankodi et al., 2000). There are several reports that CUG or CCUG repeat RNAs form nuclear foci in cells or tissues of DM1 or DM2 patients and mice expressing expanded CUG repeats by using fluorescent in situ hybridization (FISH; Taneja et al., 1995; Davis et al., 1997; Amack et al., 1999; Mankodi et al., 2000, 2001; Liquori et al., 2001). This evidence suggests that the expressions of expanded CUG or CCUG repeats are likely to be central features and sufficient for causing these symptoms.

The RNA repeat foci seem to sequester several RNA binding proteins, such as those of the well-known MBNL family (Fardaei et al., 2001, 2002; Mankodi et al., 2001). MBNL1, which has four Cys_3His zinc-finger domains, is a human homologue of *Drosophila* muscleblind (Begemann et al., 1997), which has been reported to play some role in the differentiation of eye and muscle (Begemann et al., 1997; Artero et al., 1998). MBNL1 was first isolated as a CUG repeat binding protein in relation to DM (Miller et al., 2000). Previously, the binding specificity of MBNL1 was characterized, and target RNA sequence was determined (Kino et al., 2004). The MBNLs have been established as regulators of alternative splicing (Ho et al., 2004). Recently, it was

Supplementary Material for this article is available online at http://www.mrw.interscience.wiley.com/suppmat/0360-4012/suppmat/ (www.interscience.wiley.com).

Contract grant sponsor: Ministry of Health, Labor and Welfare, Japan; Contract grant sponsor: HFSP.

*Correspondence to: Shoichi Ishiura, Department of Life Sciences, Graduate School of Arts and Sciences, University of Tokyo, Tokyo, Japan. E-mail: cishiura@mail.ecc.u-tokyo.ac.jp

Received 2 October 2007; Revised 30 November 2007; Accepted 17 December 2007

Published online 00 Month 2008 in Wiley InterScience (www.interscience.wiley.com). DOI: 10.1002/jnr.21655

suggested that *Muscleblind* has a role in translational control through a modulation of RNA stability in the cytoplasm (Houseley et al., 2005). In addition, it was shown AQ1 that localized expression of the integrin α3 is regulated at the level of RNA localization by MBNL2 (MLP1), a human paralogue of MBNL1 (Adereth et al., 2005). These findings imply that MBNL1 might also have a similar role in mRNA metabolism in the cytoplasm. The physiological functions of MBNL1 are largely unknown except that it has splicing activity and its function is down-regulated in DM. Although therapeutic strategies that restore MBNL1 function to normal would likely benefit those with DM, a broader understanding of MBNL1 function is important for elucidating DM pathogenesis.

MATERIALS AND METHODS

Plasmid Construction

The open reading frames for *YB-1*, *DDX1*, *TIA-1*, and *DCP2* were amplified by PCR from a human skeletal muscle cDNA library (Clontech, Logan, UT) and cloned into pcDNA3.1-V5 (Invitrogen, Carlsbad, CA), pECFP-C1 (Clontech), or pcDNA3-HA (Invitrogen) using conventional molecular biological techniques. $MBNL1_{40}$ was cloned into pEGFP-N1 (Clontech) or pSecDk. The pSecDk vector was generated by deleting the IgG sequence from pSecTagA (Invitrogen). The EF1-EF2 region of α-actinin was amplified by AQ1 PCR from rat genome DNA and cloned into the BglII-SalI site of pEGFP-C1 (Clontech). The nucleotide sequences of the DNA inserts were confirmed by sequencing.

Antibodies

Anti-MBNL1 rabbit polyclonal antibodies were raised using bacterially expressed $MBNL1_{40}$-6xHis as the antigen. The serum was purified with $MBNL1_{40}$-coupled Affigel 10 (Bio-Rad, Hercules, CA) and cleared by GST-6xHis-bound glutathione Separose (Amersham, Arlington Heights, IL). Goat anti-TIA-1 was purchased from Santa Cruz Biotechnology (Santa Cruz, CA). Rat anti-HA 3F10 was purchased from Roche (Indianapolis, IN). Mouse anti-V5 and anti-myc antibodies were purchased from Invitrogen. Alexa Fluor 568-labeled goat anti-mouse IgG, Alexa Fluor 488-labeled donkey anti-rabbit IgG, Alexa Fluor 546-labeled donkey anti-goat IgG, and Alexa Fluor 488-labeled donkey anti-rat IgG were purchased from Molecular Probes (Eugene, OR).

Protein Purification

Recombinant GST-$MBNL1_{40}$-6xHis was expressed in bacteria and purified as described elsewhrere (Kino et al., 2004). Briefly, pET-GX containing $MBNL1_{40}$ was transformed into BL21 (DE3) cells and cultured overnight in LB medium. The culture was then diluted and shaken at 37°C for 1.5 hr, or until the OD_{600} reached 0.3–0.4, and then 0.2 mM IPTG was added. During induction, the culture was shaken at 25°C for 4 hr. The bacterial cells were then collected and lysed twice in a French pressure cell press (Ohtake Works, Co.) before being centrifuged at 5,000*g* for 20 min. The supernatant was subjected to affinity purification using glutathione Sepharose 4B (Amersham Biosciences). The beads were washed with ATP $MgSO_4$ buffer to exclude DnaK, and GST-$MBNL1_{40}$-6xHis was eluted with 50 mM Tris-HCl, pH 8.8, and 10 mM glutathione (reduced type). The eluate was then mixed with NaCl and imidazole before the addition of Talon Metal Affinity Resin (Clontech) according to the manufacturer's protocol. Finally, the purified proteins were dialyzed against a stock buffer (50 mM Tris-HCl, pH 8.0, 100 mM NaCl, and 2 mM 2-mercaptoethanol). The quantity and purity of the samples were checked by SDS-PAGE with Coomassie brilliant blue (CBB) staining. The identity of GST-$MBNL1_{40}$-6xHis was confirmed by peptide mass fingerprinting with mass spectrometry (AXIMA-CFR; Shimadzu) following digestion with trypsin.

GST Pull-Down Assay

Mouse muscle and heart (2 g each) were homogenized in lysis buffer (50 mM Tris-HCl, pH 8.0, 100 mM NaCl, 2 mM 2-mercaptoethanol, 0.5% NP-40, 0.5% Triton X-100, and 1/1,000 vol protease inhibitors) using a Hitachi homogenizer and centrifuged at 15,000*g* for 20 min. Next, the supernatant was precleared with 500 μl of glutathione Sepharose for 2 hr and with GST-6xHis-bound glutathione Sepharose for 2 hr at 4°C. Finally, the supernatant was mixed with 20 μg of GST-$MBNL1_{40}$-6xHis and rotated overnight at 4°C. The beads were washed five times with lysis buffer, and the complex was eluted by cleavage with 3 U thrombin for 1 hr at 20°C, then subjected to SDS-PAGE.

In-Gel Trypsin Digestion and Analysis by Matrix-Assisted Laser Desorption/Ionization Tandem Time-of-Flight (MALDI-TOF/TOF) Mass Spectrometry

Pull-down assays were performed as described above. The bound proteins were separated by 12.5% SDS-PAGE and stained with Silver Quest (Invitrogen). The bands were excised from the gel and destained, dehydrated with acetonitrile for 10 min, and dried completely under a vacuum pump for 10 min. Each band was placed in 20 μl of 5 mM NH_4HCO_3 containing 1 pmol sequencing-grade trypsin (Promega, Madison, WI) at 37°C overnight. Aliquots of the trypsinized samples were analyzed by nanoliquid chromatography and automatically spotted with alfa-cyano-4-hydroxyl-cinnamic acid solution on a stainless-steel target and air dried. MALDI-TOF/TOF analysis was conducted with a Proteomics analyzer 4700 (Applied Biosystem, Foster City, CA). The proteins were identified by database searches on the web with Mascot (Matrix Science, Ltd., London, United Kingdom).

Western Blotting

The samples were subjected to 10% SDS-PAGE and transferred to PVDF membranes (Immobilon-P; Millipore, Bedford, MA). The membranes were then blocked with 5% skim milk in TPBS (0.05% Tween 20 in PBS) for 1 hr at room temperature and incubated with primary antibodies in TPBS. After washing, the membranes were incubated for 1 hr with horseradish peroxidase (HRP)-conjugated secondary antibodies. The immunoreactive bands were visualized with the LAS-3000 imaging system (Fujifilm, Tokyo, Japan).

Immunoprecipitation

COS-7 cells were transfected with myc-tagged constructs of MBNL1 and V5-tagged constructs of YB-1 or DDX1 using FuGENE6 (Roche, Basel, Switzerland). Cells from two 10-cm plates were homogenized in 500 µl lysis buffer [50 mM Tris-HCl, pH 8.0, 150 mM NaCl, 5 mM dithiothreitol (DTT), 1 mM EDTA, 1% (w/v) Triton X-100, and protease inhibitor cocktail]. The lysates were then centrifuged at 100,000*g* for 15 min at 4°C. The supernatant was precleared with protein G Sepharose 4 fast flow beads (Amersham Biosciences, Piscataway, NJ) for 1 hr and then incubated with anti-V5 antibodies fixed on beads. After the beads were washed five times with lysis buffer, the precipitates were analyzed by SDS-PAGE and immunoblotted with either anti-myc or anti-V5 antibodies.

Immunocytochemistry and Image Analysis

HeLa and COS-7 cells were fixed with PBS containing 4% (w/v) paraformaldehyde for 15 min and permeabilized with 0.1% (w/v) Triton X-100 in PBS for 15 min. After the buffer was exchanged for 3% (w/v) BSA in PBS, the cells were incubated with the first antibody in 3% BSA in PBS for 1 hr, washed with PBS, and then incubated with the second antibody in 3% BSA in PBS for 1 hr. After washing with PBS, the samples were embedded in Mowiol (Calbiochem, La Jolla, CA). Cell images were acquired on a Zeiss LSM510 Meta laser scanning confocal microscope (Carl Zeiss, Jena, Germany) or IX70 microscope (Olympus, Tokyo, Japan).

Polysome Analysis

HeLa (10-cm dish) cells were exposed to 50 µg/ml cycloheximide at 37°C for 10 min, washed twice with cold PBS, and resuspended in 300 µl TKM buffer (10 mM Tris-HCl, pH 7.5, 100 mM KCl, 5 mM $MgCl_2$, and 50 µg/ml cycloheximide). The cells were then homogenized by passing them through a 27-gauge needle 10 times. Both the PBS and the TKM contained 50 µg/ml cycloheximide. The homogenate was centrifuged at 2,000*g* for 10 min at 4°C, and the supernatant was then loaded onto a gradient of 15–40% (w/v) sucrose in TKM and sedimented for 60 min at 4°C at 40,000 rpm (18 kG) in a swinging bucket rotor. The gradient was collected in 15 fractions, with concomitant measurement of the absorbance at 254 nm. The proteins were precipitated with trichloroacetic acid and subjected to SDS-PAGE and Western blot analysis, as described above.

Splicing Assays

For the in vivo splicing assays, HEK293 cells were plated in 3.5-cm or 6-cm dishes and cultured for 24 hr in DMEM plus 10% FBS before plasmid transfection. Cells were grown to 60–80% confluence and then transiently cotransfected using FuGENE 6 (Roche) according to the manufacturer's instructions with 300 ng splicing reporter and 4 µg YB-1-V5, MBNL1-myc, or DDX1-V5. The cells were collected after 48 hr, total RNA was extracted using an RNeasy Kit (Qiagen, Valencia, CA), and the samples were analyzed by RT-PCR. Reverse-transcription was done by using PrimeScript Reverse Transcriptase (TaKaRa). Spliced products were amplified using EGFP primer (Fw: CATGGTCCTGCTGGAGTTCGTG, Rv: GTTTCAGGTTCAGGGGGAGGTGTG) and separated by 6% polyacrylamide gel.

RESULTS

Pull-Down Screening of MBNL1

MBNL1 has nine splicing isoforms (Kino et al., 2004; Pascual et al., 2006). The ratio of each isoform is likely to change during development and differentiation of muscle (Kanadia et al., 2006). Recently, it was shown that MBNL2 (MLP1) is involved in the local translation of the integrin α3 by transporting the transcript to specific points in the cytoplasm (Adereth et al., 2005). AQ1 Therefore, we focused on both the nuclear and the cytosolic compartment of MBNL1, and we selected $MBNL1_{40}$, which localizes to both compartments, for use as bait in a GST pull-down assay. Double-tagged GST-MBNL1-6xHis was purified in a two-step procedure. Purified GST-MBNL1-6xHis was bound to glutathione beads and mixed with a mouse muscle or heart lysate. After incubation overnight, the beads were washed extensively, and the proteins were eluted by thrombin cleavage. After elution, the complexes in the experimental and control samples were compared by SDS-PAGE (Fig. 1). About 20 bands were detected in F1 the sample containing muscle lysate as prey. Each band was excised from the gel and digested with trypsin. The trypsinized peptides were then subjected to MADLI-TOF/TOF analysis, and each protein was identified in MASCOT software (Suppl. Table I). Seven proteins among 20 bands were identified, and these were YB-1, DDX1, phenylalaninyl-tRNA synthetase α and β subu- AQ1 nits, amylo-1,6-glucosidase, and several small and large ribosomal subunits. YB-1 is a multifunctional RNA/DNA binding protein and has a role in transcriptional and posttranscriptional RNA metabolism, including splicing (Stickeler et al., 2001; Rapp et al., 2002; Kohno et al., 2003; Raffetseder et al., 2003; Allemand et al., 2007). DDX1 is part of the DEAD box RNA helicase family (Cordin et al., 2006). From all of the proteins identified, we focused our attention on the two proteins known to be involved in mRNA metabolism.

Interactions Between MBNL1 and YB1 or DDX1

To confirm the interaction between MBNL1 and YB-1 or DDX1, we performed a pull-down assay. Forty-eight hours after transfection with YB-1-V5 or DDX1-V5, each COS-7 lysate was mixed with GST-$MBNL1_{40}$-6xHis bound to glutathione Sepharose. After 4 hr, the beads were washed thoroughly and boiled in SDS sample buffer. The binding of these proteins was confirmed (Fig. 2A). As negative controls, RNA binding F2 proteins HuR and calreticulin were shown not to bind MBNL1 (data not shown). Next, immunoprecipitation (IP) assays were performed against MBNL1-myc and YB-1-V5 expressed in COS-7 (Fig. 2B). MBNL1-myc